

Threshold Resummation for Gaugino Pair Production at Hadron Colliders

Jonathan Debove^a, Benjamin Fuks^b, and Michael Klasen^{a*}

^a *Laboratoire de Physique Subatomique et de Cosmologie,
Université Joseph Fourier/CNRS-IN2P3/INPG, 53 Avenue des Martyrs, F-38026 Grenoble, France*

^b *Institut Pluridisciplinaire Hubert Curien/Département Recherche Subatomique,
Université de Strasbourg/CNRS-IN2P3, 23 Rue du Loess, F-67037 Strasbourg, France*

(Dated: October 28, 2018)

We present a complete analysis of threshold resummation effects on direct light and heavy gaugino pair production at the Tevatron and the LHC. Based on a new perturbative calculation at next-to-leading order of SUSY-QCD, which includes also squark mixing effects, we resum soft gluon radiation in the threshold region at leading and next-to-leading logarithmic accuracy, retaining at the same time the full SUSY-QCD corrections in the finite coefficient function. This allows us to correctly match the resummed to the perturbative cross section. Universal subleading logarithms are resummed in full matrix form. We find that threshold resummation slightly increases and considerably stabilizes the invariant mass spectra and total cross sections with respect to the next-to-leading order calculation. For future reference, we present total cross sections and their theoretical errors in tabular form for several commonly used SUSY benchmark points, gaugino pairs, and hadron collider energies.

I. INTRODUCTION

The Minimal Supersymmetric Standard Model (MSSM) [1] continues to be one of the best-motivated and most intensely studied extensions of the Standard Model (SM) of particle physics. It introduces a symmetry between fermionic and bosonic degrees of freedom in nature and predicts one fermionic (bosonic) supersymmetric (SUSY) partner for each bosonic (fermionic) SM particle. Consequently, it allows to stabilize the gap between the electroweak and the Planck scale [2] and to unify the three gauge couplings at energies of $\mathcal{O}(10^{16})$ GeV [3]. It also contains a stable lightest supersymmetric particle (LSP), which interacts only weakly and represents therefore an excellent candidate for cold dark matter [4]. Spin partners of the SM particles have not yet been observed, and in order to remain a viable solution to the hierarchy problem, SUSY must be broken at low energy via soft terms in the Lagrangian. As a consequence, the SUSY particles must be massive in comparison to their SM counterparts, and the Tevatron and the LHC will perform a conclusive search covering a wide range of masses up to the TeV scale.

The production of SUSY particles at hadron colliders has been studied at leading order (LO) of perturbative QCD since the 1980s [5]. More recently, previously neglected electroweak contributions [6], polarization effects [7], and the violation of flavor [8] and CP symmetry [9] have been considered at this order. Next-to-leading order (NLO) corrections have been computed within QCD since the late 1990s [10, 11] and recently also within the electroweak theory [12]. Resummation at the next-to-leading logarithmic (NLL) level has been achieved in the small transverse-momentum region for sleptons and gauginos [13], in the threshold region for sleptons, squarks and gluinos [14], and for sleptons and additional neutral gauge bosons also in both regions simultaneously [15].

As the fermionic partners of the electroweak gauge and Higgs bosons, the four neutralino ($\tilde{\chi}_i^0$, $i = 1, \dots, 4$) and chargino ($\tilde{\chi}_i^\pm$, $i = 1, 2$) mass eigenstates are superpositions of the neutral and charged gaugino and higgsino interaction eigenstates. Their decays into leptons and missing transverse energy, carried away by the $\tilde{\chi}_1^0$ LSP, are easily identifiable at hadron colliders. The lighter mass eigenstates are accessible not only at the LHC with center-of-mass energies \sqrt{S} of 7 to 14 TeV, but also at Run II of the Tevatron ($\sqrt{S} = 1.96$ TeV), where the production of $\tilde{\chi}_1^\pm \tilde{\chi}_2^0$ pairs decaying into trilepton final states is a gold-plated SUSY discovery channel [16]. For this particular channel, threshold resummation has been studied previously within the minimal supergravity (mSUGRA) model [17]. It was found that threshold resummation could increase the total cross section by up to 4.7% at the Tevatron relative to the NLO prediction, i.e. was significant even relatively far from the hadronic production threshold.

In this work, we extend and improve on these published results in several respects. First, we extend the original NLO calculation [11] by also including squark mixing effects. Second, we include not only the QCD, but also the SUSY-QCD virtual loop contributions in the hard coefficient function of the resummed cross section, which therefore reproduces, when expanded, the correct NLO SUSY-QCD cross section in the threshold region. Third, we resum

*klasen@lpsc.in2p3.fr

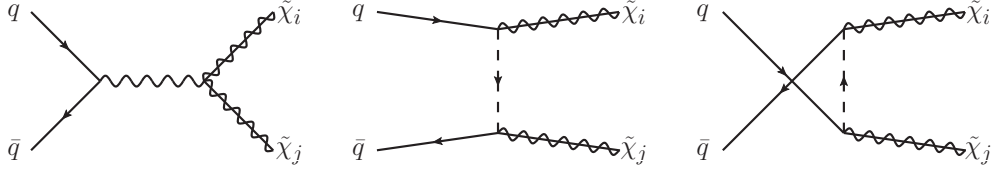


FIG. 1: Tree-level Feynman diagrams for the production of gaugino pairs.

not only the diagonal, but the full matrix contributions coming from the anomalous dimension, thereby including all universal subleading terms and full singlet mixing. However, we refrain from resumming constant terms that are known to factorize and exponentiate in Drell-Yan like processes, but not in more complex processes like gaugino pair production with several interfering Born diagrams. For the Tevatron, we consider not only the production of $\tilde{\chi}_1^\pm \tilde{\chi}_2^0$, but also of $\tilde{\chi}_2^0 \tilde{\chi}_2^0$ and $\tilde{\chi}_1^\pm \tilde{\chi}_1^\pm$ pairs. In particular the latter can have significantly larger cross sections than trilepton production due to the s -channel exchange of massless photons. For the LHC, we concentrate on predictions for its initial center-of-mass energy of $\sqrt{S} = 7$ TeV and include also the production of heavy gaugino ($\tilde{\chi}_{2,3,4}^\pm, \tilde{\chi}_{3,4}^0$) combinations, where threshold effects and direct gaugino pair production (as opposed to the production from squark and gluino cascade decays) will be more important. However, we will also show cross sections for $\sqrt{S} = 14$ TeV for comparison.

The remainder of this paper is organized as follows: In Sec. II, we present briefly our LO and NLO SUSY-QCD calculations, focusing on squark mixing, the ultraviolet renormalization procedure and the dipole subtraction method employed for the cancellation of infrared divergences among virtual and real contributions. In Sec. III, we describe the threshold resummation formalism in Mellin space, starting from the refactorization of the perturbative cross section and the exponentiation of the eikonal function, giving then the explicit form of the resummed logarithms at NLL order, and finally describing various ways to improve on the original formalism. Sec. IV contains numerical results for various gaugino pair production cross sections at the Tevatron and at the LHC in both graphical and tabular form. It also includes a comprehensive analysis of theoretical errors coming from scale and parton density uncertainties. We summarize our results in Sec. V. Our conventions for the couplings of quarks and squarks to weak gauge bosons and gauginos are defined in the Appendix.

II. GAUGINO PAIR PRODUCTION AT FIXED ORDER IN PERTURBATIVE QCD

At hadron colliders, two gauginos $\tilde{\chi}_{i,j}$ with masses $m_{\tilde{\chi}_{i,j}}$ and four-momenta $p_{1,2}$ can be produced at LO of perturbation theory only through the annihilation of quarks q and antiquarks \bar{q}' with four-momenta $p_{a,b}$,

$$q(p_a) \bar{q}'(p_b) \rightarrow \tilde{\chi}_i(p_1) \tilde{\chi}_j(p_2), \quad (1)$$

since gluons couple neither to electroweak gauge/Higgs bosons nor to their SUSY partners [43]. As shown in Fig. 1, the production can proceed either through the s -channel exchange of a photon (γ), neutral (Z) or charged (W) weak gauge boson, depending on the charge of the final state, or through the t - and u -channel exchange of a squark (\tilde{q}), where the Mandelstam variables

$$s = (p_a + p_b)^2, \quad t = (p_a - p_1)^2, \quad \text{and} \quad u = (p_a - p_2)^2 \quad (2)$$

and their mass-subtracted counterparts $t_{\tilde{\chi}_{i,j}} = t - m_{\tilde{\chi}_{i,j}}^2$ and $u_{\tilde{\chi}_{i,j}} = u - m_{\tilde{\chi}_{i,j}}^2$ are defined in the usual way.

A. Leading order cross section

The LO differential cross section for given (anti-)quark helicities $h_{a,b}$ can be expressed in the compact form

$$\frac{d\sigma_{q\bar{q}'}^{h_a, h_b}}{dt} = \frac{4\pi\alpha^2}{C_A(1 + \delta_{\chi_i\chi_j})x_W^2 s^2} \left\{ (1 - h_a)(1 + h_b) \left[|Q_{LL}^u|^2 u_{\tilde{\chi}_i} u_{\tilde{\chi}_j} + |Q_{LL}^t|^2 t_{\tilde{\chi}_i} t_{\tilde{\chi}_j} + 2\text{Re}[Q_{LL}^{u*} Q_{LL}^t] m_{\tilde{\chi}_i} m_{\tilde{\chi}_j} s \right] \right. \quad (3)$$

$$+ (1 + h_a)(1 - h_b) \left[|Q_{RR}^u|^2 u_{\tilde{\chi}_i} u_{\tilde{\chi}_j} + |Q_{RR}^t|^2 t_{\tilde{\chi}_i} t_{\tilde{\chi}_j} + 2\text{Re}[Q_{RR}^{u*} Q_{RR}^t] m_{\tilde{\chi}_i} m_{\tilde{\chi}_j} s \right]$$

$$+ (1 + h_a)(1 + h_b) \left[|Q_{RL}^u|^2 u_{\tilde{\chi}_i} u_{\tilde{\chi}_j} + |Q_{RL}^t|^2 t_{\tilde{\chi}_i} t_{\tilde{\chi}_j} - 2\text{Re}[Q_{RL}^{u*} Q_{RL}^t] (ut - m_{\tilde{\chi}_i}^2 m_{\tilde{\chi}_j}^2) \right]$$

$$\left. + (1 - h_a)(1 - h_b) \left[|Q_{LR}^u|^2 u_{\tilde{\chi}_i} u_{\tilde{\chi}_j} + |Q_{LR}^t|^2 t_{\tilde{\chi}_i} t_{\tilde{\chi}_j} - 2\text{Re}[Q_{LR}^{u*} Q_{LR}^t] (ut - m_{\tilde{\chi}_i}^2 m_{\tilde{\chi}_j}^2) \right] \right\}$$

TABLE I: s -channel charges for gaugino pair production. The masses of the W - and Z -bosons are m_W and m_Z .

	Q_L^{su}	Q_L^{st}	Q_R^{su}	Q_R^{st}
$\tilde{\chi}_i^0 \tilde{\chi}_j^0$	$\frac{L_{qq'Z} O_{ij}^{\prime L}}{s-m_Z^2}$	$\frac{L_{qq'Z} O_{ij}^{\prime R}}{s-m_Z^2}$	$\frac{R_{qq'Z} O_{ij}^{\prime R}}{s-m_Z^2}$	$\frac{R_{qq'Z} O_{ij}^{\prime L}}{s-m_Z^2}$
$\tilde{\chi}_i^+ \tilde{\chi}_j^0$	$\frac{L_{qq'W}^* O_{ji}^{L*}}{s-m_W^2}$	$\frac{L_{qq'W}^* O_{ji}^{R*}}{s-m_W^2}$	0	0
$\tilde{\chi}_i^+ \tilde{\chi}_j^-$	$-\frac{e_q x_W \delta_{qq'} \delta_{ij}}{4s} + \frac{L_{qq'Z} O_{ij}^{\prime L}}{s-m_Z^2}$	$-\frac{e_q x_W \delta_{qq'} \delta_{ij}}{4s} + \frac{L_{qq'Z} O_{ij}^{\prime R}}{s-m_Z^2}$	$-\frac{e_q x_W \delta_{qq'} \delta_{ij}}{4s} + \frac{R_{qq'Z} O_{ij}^{\prime R}}{s-m_Z^2}$	$-\frac{e_q x_W \delta_{qq'} \delta_{ij}}{4s} + \frac{R_{qq'Z} O_{ij}^{\prime L}}{s-m_Z^2}$

by employing the generalized charges

$$Q_{XY}^t = 2Q_X^t \delta_{XY} - \sum_{\bar{q}} \frac{X_{\bar{q}q}^* Y_{q\bar{q}} \tilde{\chi}_j}{t-m_{\bar{q}}^2} \quad \text{and} \quad Q_{XY}^u = 2Q_X^u \delta_{XY} + \sum_{\bar{q}} \frac{X_{\bar{q}q}^* Y_{q\bar{q}} \tilde{\chi}_i}{u-m_{\bar{q}}^2}, \quad (4)$$

where the s -channel charges Q_X^{st} and Q_X^{su} are given in Tab. I, $m_{\bar{q}}$ is the mass of the squark exchanged in the t - or u -channel, $X, Y \in \{L, R\}$ relate to the left- and right-handed (s)quark couplings to weak gauge bosons and gauginos listed in App. A, and the couplings of the latter among each other depend on the neutral and charged gaugino-higgsino mixing matrices N , U and V through the bilinear combinations [1]

$$O_{ij}^L = \frac{1}{2\sqrt{2}} N_{i4} V_{j2}^* - \frac{1}{2} N_{i2} V_{j1}^* \quad \text{and} \quad O_{ij}^R = -\frac{1}{2\sqrt{2}} N_{i3}^* U_{j2} - \frac{1}{2} N_{i2}^* U_{j1}, \quad (5)$$

$$O_{ij}^{L'} = \frac{1}{2c_W} V_{i1} V_{j1}^* + \frac{1}{4c_W} V_{i2} V_{j2}^* - \frac{1}{2c_W} \delta_{ij} x_W \quad \text{and} \quad O_{ij}^{R'} = \frac{1}{2c_W} U_{i1}^* U_{j1} + \frac{1}{4c_W} U_{i2}^* U_{j2} - \frac{1}{2c_W} \delta_{ij} x_W, \quad (6)$$

$$O_{ij}^{\prime L} = \frac{1}{4c_W} [N_{i3} N_{j3}^* - N_{i4} N_{j4}^*] \quad \text{and} \quad O_{ij}^{\prime R} = \frac{1}{4c_W} [-N_{i3}^* N_{j3} + N_{i4}^* N_{j4}]. \quad (7)$$

$\alpha = e^2/(4\pi)$ is the electromagnetic fine structure constant, $x_W = 1 - c_W^2 = s_W^2 = \sin^2 \theta_W$ is the squared sine of the electroweak mixing angle, and $C_A = 3$, $C_F = 4/3$ and $\alpha_s = g_s^2/(4\pi)$ are the QCD color factors and coupling constant. Unpolarized cross sections are obtained by averaging the polarized ones with

$$d\sigma_{q\bar{q}'}^{(0)} = \frac{d\sigma_{q\bar{q}'}^{1,1} + d\sigma_{q\bar{q}'}^{1,-1} + d\sigma_{q\bar{q}'}^{-1,1} + d\sigma_{q\bar{q}'}^{-1,-1}}{4}. \quad (8)$$

B. Virtual corrections

At NLO of SUSY-QCD, $\mathcal{O}(\alpha_s)$, the cross section for gaugino pair production receives contributions from the interference of the virtual one-loop diagrams shown in Figs. 2–4 with the tree-level diagrams shown in Fig. 1 on the one hand and from real gluon (Fig. 5) and (anti-)quark emission diagrams on the other hand, where the latter are obtained by crossing the final-state gluon in Fig. 5 with the initial-state antiquark (Fig. 6) or quark (not shown). All diagrams have been evaluated analytically with self-written FORM programs and cross-checked independently with self-written MATHEMATICA programs.

The virtual self-energy diagrams for left- and right-handed quarks $q_{L,R} = P_{L,R} q = \frac{1}{2}(1 \mp \gamma_5)q$ (Fig. 2, third line),

$$\Sigma_{L,R}^{(g)}(p) = -\frac{g_s^2 C_F}{16\pi^2} [(D-2)\not{p} B_1(p, m_q, 0) + D m_q B_0(p, m_q, 0)] P_{L,R}, \quad (9)$$

$$\Sigma_L^{(\tilde{g})}(p) = -\frac{g_s^2 C_F}{8\pi^2} \sum_{i=1}^2 [\not{p} B_1(p, m_{\tilde{g}}, m_{\tilde{q}_i}) R_{i1}^{\tilde{q}*} R_{i1}^{\tilde{q}} + m_{\tilde{g}} B_0(p, m_{\tilde{g}}, m_{\tilde{q}_i}) R_{i2}^{\tilde{q}*} R_{i1}^{\tilde{q}}] P_L, \quad \text{and} \quad (10)$$

$$\Sigma_R^{(\tilde{g})}(p) = -\frac{g_s^2 C_F}{8\pi^2} \sum_{i=1}^2 [\not{p} B_1(p, m_{\tilde{g}}, m_{\tilde{q}_i}) R_{i2}^{\tilde{q}*} R_{i2}^{\tilde{q}} + m_{\tilde{g}} B_0(p, m_{\tilde{g}}, m_{\tilde{q}_i}) R_{i1}^{\tilde{q}*} R_{i2}^{\tilde{q}}] P_R, \quad (11)$$

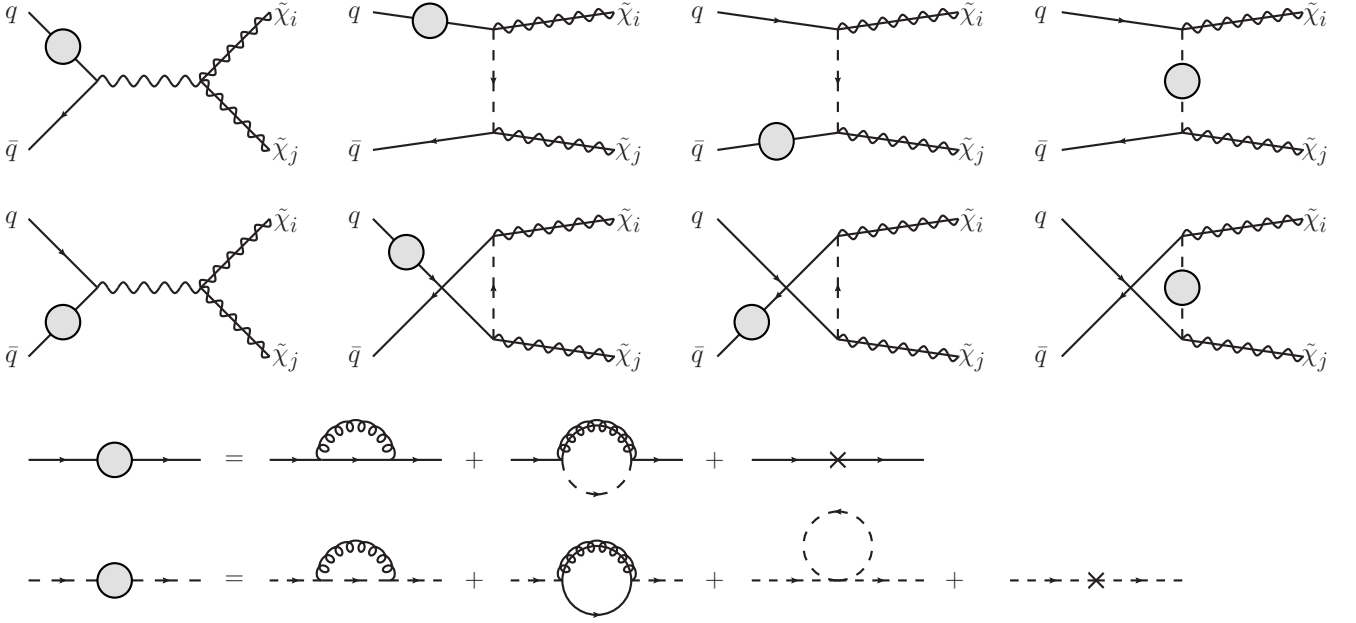


FIG. 2: Self-energy insertions (top) and contributions (bottom) to the production of gaugino pairs.

expanded as usual into vector (V) and scalar (S) parts $\Sigma(p) = [\Sigma_L^V(p^2)\not{p} + \Sigma_L^S(p^2)]P_L + (L \leftrightarrow R)$, as well as those for squarks (Fig. 2, fourth line),

$$\Sigma_{ij}^{(g)}(p^2) = -\frac{g_s^2 C_F}{16\pi^2} \left[p^2 (B_0(p, m_{\tilde{q}_i}, 0) - 2B_1(p, m_{\tilde{q}_i}, 0) + B_{21}(p, m_{\tilde{q}_i}, 0)) + DB_{22}(p, m_{\tilde{q}_i}, 0) \right] \delta_{ij}, \quad (12)$$

$$\Sigma_{ij}^{(\tilde{g})}(p^2) = -\frac{g_s^2 C_F}{4\pi^2} \left\{ \left[p^2 (B_1(p, m_q, m_{\tilde{g}}) + B_{21}(p, m_q, m_{\tilde{g}})) + DB_{22}(p, m_q, m_{\tilde{g}}) \right] \delta_{ij} - m_q m_{\tilde{g}} B_0(p, m_q, m_{\tilde{g}}) (R_{i1}^{\tilde{q}} R_{j2}^{\tilde{q}*} + R_{i2}^{\tilde{q}} R_{j1}^{\tilde{q}*}) \right\}, \quad \text{and} \quad (13)$$

$$\Sigma_{ij}^{(\tilde{q})}(p^2) = \frac{g_s^2 C_F}{16\pi^2} \sum_{k=1}^2 S_{ki}^{\tilde{q}} S_{kj}^{\tilde{q}*} A_0(m_{\tilde{q}_k}) \quad \text{with} \quad S_{ki} = R_{k1}^{\tilde{q}*} R_{i1}^{\tilde{q}} - R_{k2}^{\tilde{q}*} R_{i2}^{\tilde{q}}, \quad (14)$$

contain ultraviolet (UV) divergences in the scalar integrals $B_{0,1,\dots}(p, m_1, m_2)$ [18], which exhibit themselves as $1/\epsilon$ poles in $D = 4 - 2\epsilon$ dimensions [44]. They must therefore be absorbed through a suitable renormalization procedure into the fundamental wave functions, mass parameters, and coupling constants of the SUSY-QCD Lagrangian

$$\mathcal{L} = \left[\tilde{q}_L^0 i \not{\partial} \tilde{q}_L^0 - \tilde{q}_R^0 m_q^0 \tilde{q}_L^0 + (L \leftrightarrow R) \right] + \left[\sum_{i=1}^2 (\partial_\mu \tilde{q}_i^0)^\dagger (\partial^\mu \tilde{q}_i^0) - \tilde{q}_i^{0\dagger} (m_{\tilde{q}}^2)_{ii}^0 \tilde{q}_i^0 \right] + \dots \quad (15)$$

The two components of the unrenormalized squark field \tilde{q}^0 correspond originally to the left- and right-handed chiralities of the unrenormalized SM quark field q^0 , but mix due to the fact that soft SUSY-breaking and Higgs terms render the 2×2 -dimensional mass matrix $(m_{\tilde{q}}^2)^0$ non-diagonal [1]. In Eq. (15) we have diagonalized this mass matrix with the squark rotation matrix $R^{\tilde{q}^0}$, so that the components $i = 1(2)$ of the squark field correspond to the squark mass eigenvalues $m_{\tilde{q}_i}^0$. The squark self-energies in Eqs. (12)-(14) thus also carry indices $i, j = 1, 2$ corresponding to the (outgoing and incoming) squark mass eigenstates. Multiplicative renormalization is achieved perturbatively by expanding the renormalization constants,

$$q_{L,R}^0 = \left(1 + \frac{1}{2} \delta Z_q \right) q_{L,R} \quad \text{and} \quad m_q^0 = m_q + \delta m_q, \quad (16)$$

$$\tilde{q}_i^0 = \left(\delta_{ij} + \frac{1}{2} \delta Z_{\tilde{q},ij} \right) \tilde{q}_j \quad \text{and} \quad (m_{\tilde{q}}^2)_{ij}^0 = (m_{\tilde{q}}^2)_{ij} + (\delta m_{\tilde{q}}^2)_{ij}, \quad (17)$$

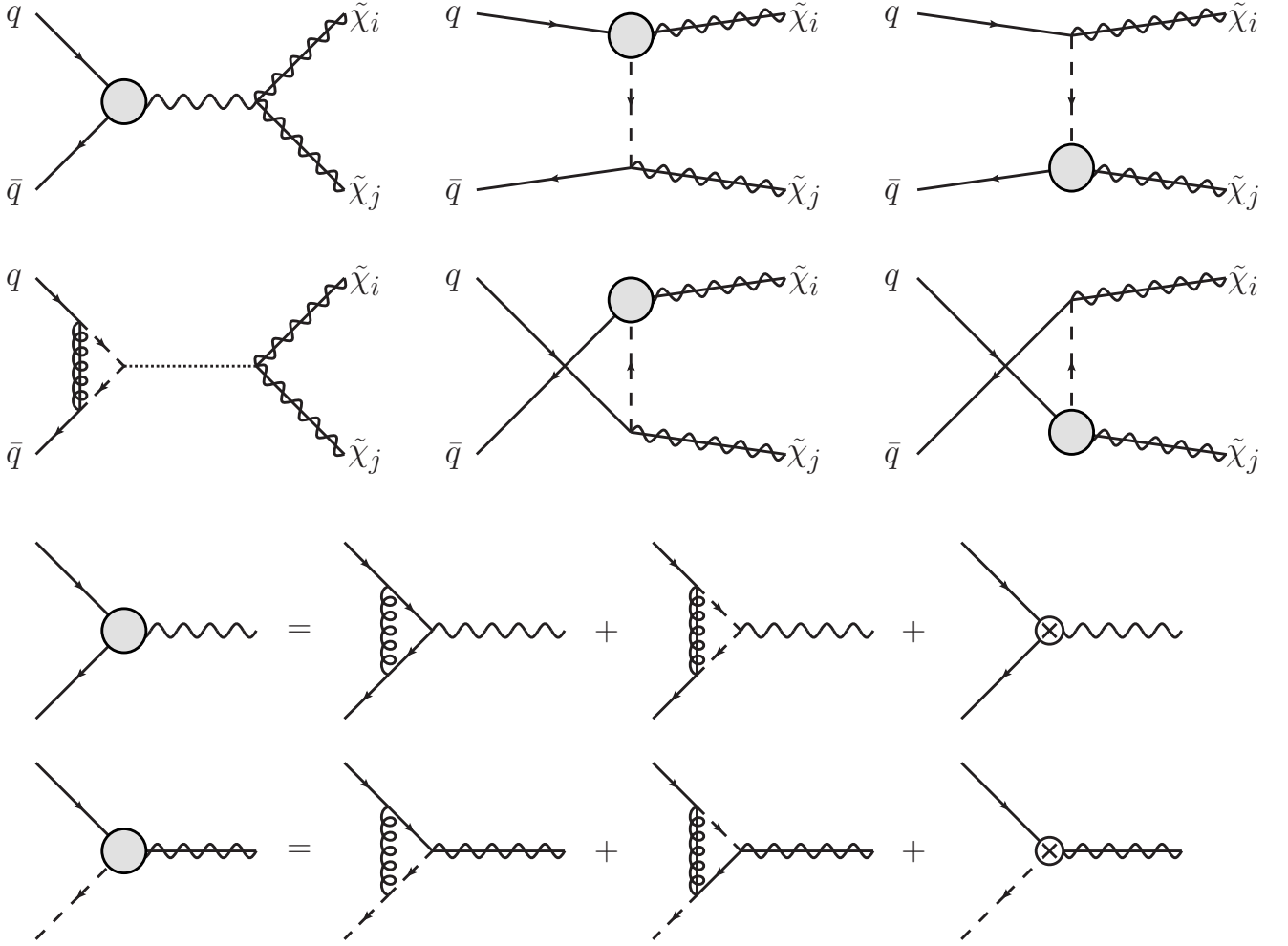


FIG. 3: Vertex correction insertions (top) and contributions (bottom) to the production of gaugino pairs.

with the usual factor of 1/2 for the (s)quark wave functions. The renormalized self-energies are then

$$\hat{\Sigma}(p) = \left[\Sigma_L^V(p^2) + \frac{1}{2}(\delta Z_q + \delta Z_q^\dagger) \right] \not{p} P_L + \left[\Sigma_L^S(p^2) - \frac{1}{2}(m_q \delta Z_q + \delta Z_q^\dagger m_q) - \delta m_q \right] P_L + (L \leftrightarrow R) \quad (18)$$

for quarks and

$$\hat{\Sigma}_{ij}(p^2) = \Sigma_{ij}(p^2) + \frac{1}{2}(\delta Z_{\tilde{q},ij} + \delta Z_{\tilde{q},ji}^*) p^2 - \frac{1}{2} \sum_{k=1}^2 \left[(m_{\tilde{q}}^2)_{ik} \delta Z_{\tilde{q},kj} + \delta Z_{\tilde{q},ki}^* (m_{\tilde{q}}^2)_{kj} \right] - (\delta m_{\tilde{q}}^2)_{ij} \quad (19)$$

for squarks.

We choose to renormalize the wave functions in the $\overline{\text{MS}}$ -scheme, so that the definition of the quark fields corresponds to the one employed in the parton densities in the external hadrons [45]. In this scheme, the quark wave function counterterm

$$\delta Z_q = \delta Z_q^{(g)} + \delta Z_q^{(\tilde{g})} \quad \text{with} \quad \delta Z_q^{(g)} = \delta Z_q^{(\tilde{g})} = -\frac{g_s^2 C_F}{16\pi^2} \Delta \quad \text{and} \quad \Delta = \frac{1}{\epsilon} - \gamma_E + \ln 4\pi, \quad (20)$$

defined as the UV-divergent plus universal finite parts of the on-shell counterterm $-\Sigma_{L,R}^V(m_q^2) - m_q^2[\Sigma_{L,R}^{V'}(m_q^2) + \Sigma_{R,L}^{V'}(m_q^2)] - m_q[\Sigma_{L,R}^{S'}(m_q^2) + \Sigma_{R,L}^{S'}(m_q^2)]$ [19], is hermitian ($\delta Z_q = \delta Z_q^\dagger$) and the same for left- and right-handed quarks. The superscripts g and \tilde{g} label the gluon and gluino exchange contributions, respectively, and γ_E is the Euler constant. The squark wave function counterterms

$$\delta Z_{\tilde{q},ij} = \delta Z_{\tilde{q},ij}^{(g)} + \delta Z_{\tilde{q},ij}^{(\tilde{g})} + \delta Z_{\tilde{q},ij}^{(\tilde{q})}, \quad (21)$$

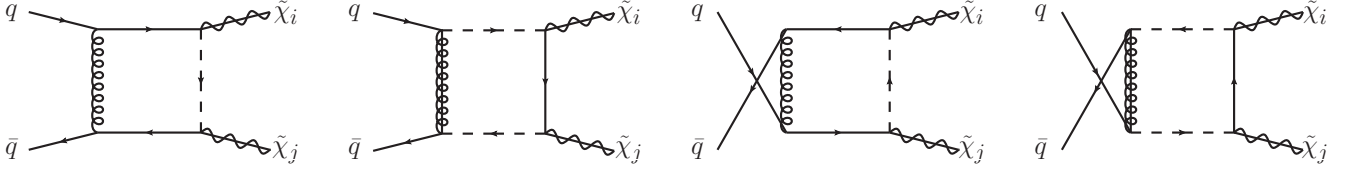


FIG. 4: Box diagrams contributing to the production of gaugino pairs at NLO.

with

$$\delta Z_{\bar{q},ii}^{(g)} = -\delta Z_{\bar{q},ii}^{(\bar{g})} = \frac{g_s^2 C_F}{8\pi^2} \Delta \quad \text{and} \quad \delta Z_{\bar{q},ii}^{(\bar{q})} = 0 \quad (22)$$

for $i = j$ and

$$\delta Z_{\bar{q},ij}^{(g)} = 0, \quad (23)$$

$$\delta Z_{\bar{q},ij}^{(\bar{g})} = \frac{g_s^2 C_F}{4\pi^2} \frac{2\Delta}{m_{\bar{q}_i}^2 - m_{\bar{q}_j}^2} \left[m_q m_{\bar{g}} (R_{i1}^{\bar{q}} R_{j2}^{\bar{q}*} + R_{i2}^{\bar{q}} R_{j1}^{\bar{q}*}) \right], \quad \text{and} \quad (24)$$

$$\delta Z_{\bar{q},ij}^{(\bar{q})} = \frac{g_s^2 C_F}{16\pi^2} \frac{2\Delta}{m_{\bar{q}_i}^2 - m_{\bar{q}_j}^2} \sum_{k=1}^2 m_{\bar{q}_k}^2 S_{ki} S_{kj}^* \quad (25)$$

for $i \neq j$, defined similarly as the UV-divergent plus universal finite parts of the on-shell counterterms $-\widetilde{\text{Re}} \Sigma'_{ii}(m_{\bar{q}_i}^2)$ for $i = j$ and $2 \widetilde{\text{Re}} \Sigma_{ij}(m_{\bar{q}_j}^2)/(m_{\bar{q}_i}^2 - m_{\bar{q}_j}^2)$ for $i \neq j$ [19], enter only through the renormalization of the squark mixing matrix,

$$R^{\bar{q}0} = R^{\bar{q}} + \delta R^{\bar{q}} \quad \text{with} \quad \delta R_{ij}^{\bar{q}} = \frac{1}{4} \sum_{k=1}^2 (\delta Z_{\bar{q},ik} - \delta Z_{\bar{q},ki}^*) R_{kj}^{\bar{q}} = \frac{1}{2} \sum_{k=1}^2 \delta Z_{\bar{q},ik} R_{kj}^{\bar{q}}, \quad (26)$$

since in the $\overline{\text{MS}}$ -scheme the gluon and gluino contributions for $i = j$ in Eq. (22) cancel each other. In the last step of Eq. (26), we have made use of the fact that in the $\overline{\text{MS}}$ -scheme the squark wave-function renormalization constants are anti-hermitian matrices ($\delta Z_{\bar{q},ij} = -\delta Z_{\bar{q},ji}^*$).

The (s)quark masses are renormalized in the on-shell scheme to make them correspond to the physical masses. The quark mass counterterm is then defined by $m_q \Sigma^V(m_q^2) + \Sigma^S(m_q^2)$ [19] with the result

$$\delta m_q = \delta m_q^{(g)} + \delta m_q^{(\bar{g})} \quad (27)$$

and

$$\delta m_q^{(g)} = -\frac{g_s^2 C_F}{16\pi^2} m_q \left[(D-2)B_1(m_q, m_q, 0) + DB_0(m_q, m_q, 0) \right], \quad (28)$$

$$\delta m_q^{(\bar{g})} = -\frac{g_s^2 C_F}{16\pi^2} \sum_{i=1}^2 \left[m_q B_1(m_q, m_{\bar{g}}, m_{\bar{q}_i}) + 2m_{\bar{g}} B_0(m_q, m_{\bar{g}}, m_{\bar{q}_i}) \text{Re}(R_{i2}^{\bar{q}*} R_{i1}^{\bar{q}}) \right]. \quad (29)$$

For our numerical results, we will set the masses of external quarks to zero in accordance with the collinear factorization of quarks in hadrons. The squark mass counterterm is defined by $\widetilde{\text{Re}}[\Sigma_{ii}(m_{\bar{q}_i}^2)]$. The result is

$$\delta m_{\bar{q}_i}^2 = \delta m_{\bar{q}_i}^{2(g)} + \delta m_{\bar{q}_i}^{2(\bar{g})} + \delta m_{\bar{q}_i}^{2(\bar{q})} \quad (30)$$

with

$$\delta m_{\bar{q}_i}^{2(g)} = \frac{g_s^2 C_F}{8\pi^2} m_{\bar{q}_i}^2 \left[B_1(m_{\bar{q}_i}, m_{\bar{q}_i}, 0) - B_0(m_{\bar{q}_i}, m_{\bar{q}_i}, 0) \right], \quad (31)$$

$$\delta m_{\bar{q}_i}^{2(\bar{g})} = -\frac{g_s^2 C_F}{4\pi^2} \left[m_{\bar{q}_i}^2 B_1(m_{\bar{q}_i}, m_q, m_{\bar{g}}) + m_q^2 B_0(m_{\bar{q}_i}, m_q, m_{\bar{g}}) + A_0(m_{\bar{g}}) \right. \\ \left. - 2m_q m_{\bar{g}} B_0(m_{\bar{q}_i}, m_q, m_{\bar{g}}) \text{Re}(R_{i1}^{\bar{q}} R_{i2}^{\bar{q}*}) \right], \quad \text{and} \quad (32)$$

$$\delta m_{\bar{q}_i}^{2(\bar{q})} = \frac{g_s^2 C_F}{16\pi^2} \sum_{j=1}^2 |S_{ji}|^2 A_0(m_{\bar{q}_j}). \quad (33)$$

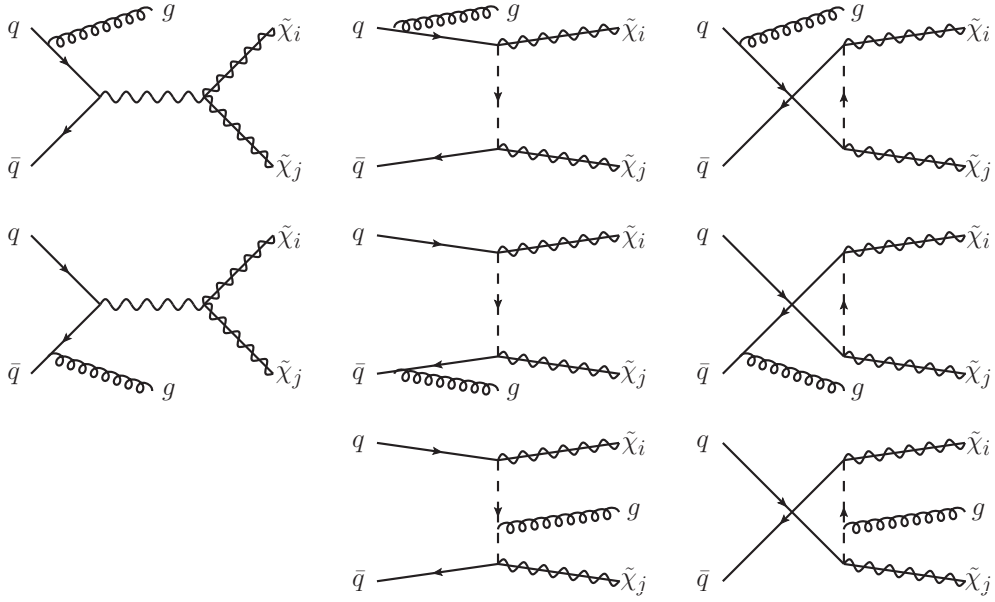


FIG. 5: Gluon emission diagrams contributing to the production of gaugino pairs at NLO.

Supersymmetric Ward identities link the quark-quark-gauge boson and quark-squark-gaugino vertices to the weak gauge-boson and gaugino self-energies. As the latter do not receive strong corrections at NLO, the former require no further renormalization beyond the one for the (s)quark wave functions discussed above. However, the artificial breaking of supersymmetry by the mismatch of two gaugino and $(D - 2)$ transverse vector degrees of freedom must be compensated by a finite counterterm $\hat{g} = g[1 - \alpha_s C_F / (8\pi)]$, effectively shifting the quark-squark-gaugino scalar coupling constant \hat{g} with respect to the weak gauge coupling constant g [10, 20].

C. Real corrections

Apart from the (now UV-finite) virtual corrections $d\sigma_{ab}^{(V)}$ to the LO cross section $d\sigma_{ab}^{(0)}$ described above, the NLO cross section

$$\begin{aligned}
d\sigma_{ab}^{(1)}(p_a, p_b) &= \int_{2+1} \left[\left(d\sigma_{ab}^{(R)}(p_a, p_b) \right)_{\epsilon=0} - \left(\sum_{\text{dipoles}} d\sigma_{ab}^{(0)}(p_a, p_b) \otimes dV_{\text{dipole}} \right)_{\epsilon=0} \right] \\
&+ \int_2 \left[d\sigma_{ab}^{(V)}(p_a, p_b) + d\sigma_{ab}^{(0)}(p_a, p_b) \otimes \mathbf{I} \right]_{\epsilon=0} \\
&+ \sum_{a'} \int_0^1 dx \int_2 \left[d\sigma_{a'b}^{(0)}(xp_a, p_b) \otimes (\mathbf{P} + \mathbf{K})^{a,a'}(x) + d\sigma_{aa'}^{(0)}(p_a, xp_b) \otimes (\mathbf{P} + \mathbf{K})^{b,a'}(x) \right]_{\epsilon=0} \quad (34)
\end{aligned}$$

also receives contributions $d\sigma_{ab}^{(R)}$ from real gluon (Fig. 5), quark (Fig. 6) and antiquark (not shown) emission diagrams, where the emitted parton carries four-momentum p_3 . In the Catani-Seymour dipole formalism [21], the real contributions are rendered infrared (IR) finite by subtracting from them their soft and collinear limits ($p_{a,b} \cdot p_3 \rightarrow 0$)

$$d\sigma_{ab}^{(0)}(p_a, p_b) \otimes dV_{\text{dipole}} = \sum_i \left[\mathcal{D}^{a3,b}(p_1, p_2, p_3; p_a, p_b) F_J^{(2)}(\tilde{p}_1, \tilde{p}_2; \tilde{p}_{a3}, p_b) + (a \leftrightarrow b) \right] \quad (35)$$

before integration over the three-particle final-state phase space. They can then be evaluated in four dimensions (i.e. with $\epsilon = 0$). In the case at hand of two initial-state partons and no colored final state particles at LO, the only dipole contribution comes from an initial state emitter and an initial state spectator, e.g.

$$\mathcal{D}^{a3,b}(p_1, p_2, p_3; p_a, p_b) = -\frac{1}{2p_a \cdot p_3} \frac{1}{x_{3,ab}} {}_{2,ab} \langle \tilde{1}, \tilde{2}; \tilde{a3}, b | \frac{\mathbf{T}_b \cdot \mathbf{T}_{a3}}{\mathbf{T}_{a3}^2} \mathbf{V}^{a3,b} | \tilde{1}, \tilde{2}; \tilde{a3}, b \rangle_{2,ab} \quad (36)$$

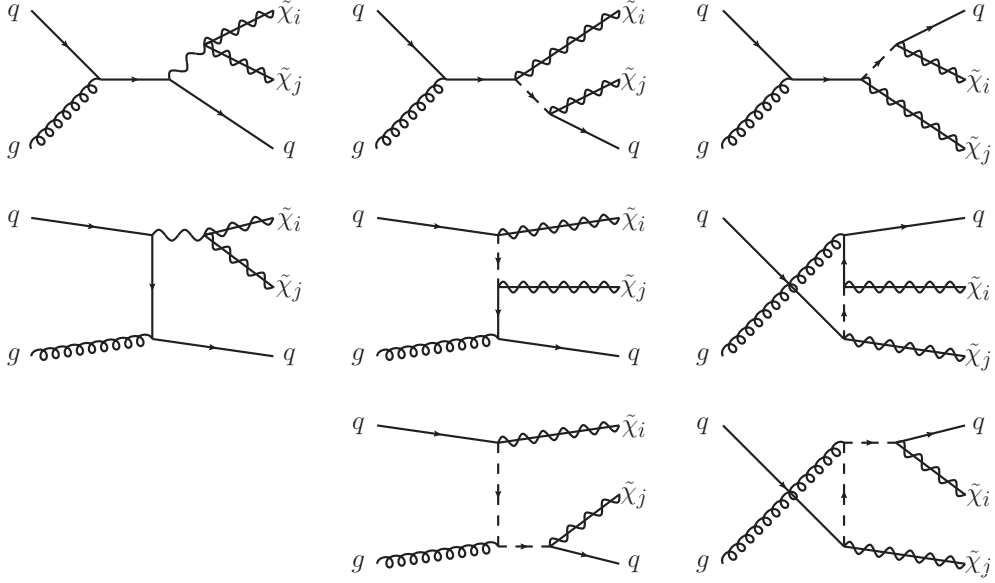


FIG. 6: Quark emission diagrams contributing to the production of gaugino pairs at NLO.

(see Eq. (5.136) of Ref. [21]). The color charges $\mathbf{T}_{a3,b}$ and splitting functions $\mathbf{V}^{a3,b}$ (Eqs. (5.145)-(5.148) of Ref. [21]) act on Born-like squared matrix elements, which are written here in terms of vectors $[\tilde{1}, \tilde{2}; \tilde{a3}, b]_{2,ab}$ in color and helicity space. These matrix elements involve an initial-state parton $\tilde{a3}$ with momentum parallel to p_a ,

$$\tilde{p}_{a3}^\mu = x_{3,ab} p_a^\mu, \quad \text{where} \quad x_{3,ab} = \frac{p_a \cdot p_b - p_3 \cdot p_a - p_3 \cdot p_b}{p_a \cdot p_b}, \quad (37)$$

and rescaled four-momenta of the final-state gauginos

$$\tilde{p}_{1,2}^\mu = p_{1,2}^\mu - \frac{2p_{1,2} \cdot (K + \tilde{K})}{(K + \tilde{K})^2} (K + \tilde{K})^\mu + \frac{2p_{1,2} \cdot K}{K^2} \tilde{K}^\mu, \quad (38)$$

where $K^\mu = p_a^\mu + p_b^\mu - p_3^\mu$ and $\tilde{K}^\mu = \tilde{p}_{a3}^\mu + p_b^\mu$. The phase space function $F_J^{(2)}(\tilde{p}_1, \tilde{p}_2; \tilde{p}_{a3}, p_b)$ tends to zero with $p_a \cdot p_3$ and ensures therefore that the LO cross section is IR-finite. To compensate for the subtracted auxiliary dipole term $d\sigma_{ab}^{(0)}(p_a, p_b) \otimes dV_{\text{dipole}}$, the latter must be integrated analytically over the full phase space of the emitted parton,

$$\mathbf{I} = \sum_{\text{dipoles}} \int_1 dV_{\text{dipole}}, \quad (39)$$

and added to the virtual cross section. The integrated dipole term is defined explicitly in Eq. (10.15) of Ref. [21]; it contains all the simple and double poles in ϵ necessary to cancel the IR singularities in $d\sigma_{ab}^{(V)}$. The insertion operators

$$\mathbf{P}^{a,a'}(p_1, \dots, p_m, p_b; xp_a, x; \mu_F^2) = \frac{\alpha_s}{2\pi} P^{aa'}(x) \frac{1}{\mathbf{T}_{a'}^2} \left[\sum_i \mathbf{T}_i \cdot \mathbf{T}_{a'} \ln \frac{\mu_F^2}{2xp_a \cdot p_i} + \mathbf{T}_b \cdot \mathbf{T}_{a'} \ln \frac{\mu_F^2}{2xp_a \cdot p_b} \right] \quad (40)$$

are directly related to the regularized Altarelli-Parisi splitting distributions at $\mathcal{O}(\alpha_s)$,

$$P^{qq}(x) = C_F \left[\frac{1+x^2}{(1-x)_+} + \frac{3}{2} \delta(1-x) \right], \quad (41)$$

$$P^{qg}(x) = C_F \left[\frac{1+(1-x)^2}{x} \right], \quad (42)$$

$$P^{gq}(x) = T_R [x^2 + (1-x)^2], \quad \text{and} \quad (43)$$

$$P^{gg}(x) = 2C_A \left[\left(\frac{1}{1-x} \right)_+ + \frac{1-x}{x} - 1 + x(1-x) \right] + \beta_0 \delta(1-x), \quad (44)$$

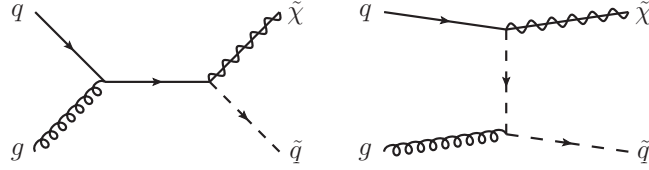


FIG. 7: Associated production of a gaugino and a virtual squark, decaying subsequently into a gaugino and a quark.

where $\beta_0 = 11C_A/6 - 2N_f T_R/3$ and $\beta_1 = (17C_A^2 - 5C_A N_f - 3C_F N_f)/6$ are the one- and two-loop coefficients of the QCD beta-function, $C_F = 4/3$, $T_R = 1/2$, $C_A = 3$, and N_f is the number of quark flavors. They cancel the dependence of the hadronic cross section on the factorization scale μ_F up to NLO accuracy. The insertion operators

$$\mathbf{K}^{a,a'}(x) = \frac{\alpha_s}{2\pi} \left\{ \overline{K}^{aa'}(x) - K_{\text{F.S.}}^{aa'}(x) + \delta^{aa'} \sum_i \mathbf{T}_i \cdot \mathbf{T}_a \frac{\gamma_i^{(1)}}{\mathbf{T}_i^2} \left[\left(\frac{1}{1-x} \right)_+ + \delta(1-x) \right] \right\} - \frac{\alpha_s}{2\pi} \mathbf{T}_b \cdot \mathbf{T}_{a'} \frac{1}{\mathbf{T}_{a'}^2} \tilde{K}^{aa'}(x) \quad (45)$$

with $\gamma_q^{(1)} = 3C_F/2$ and $\gamma_g^{(1)} = \beta_0$,

$$\overline{K}^{qq}(x) = \overline{K}^{\bar{q}\bar{q}}(x) = C_F \left[\left(\frac{2}{1-x} \ln \frac{1-x}{x} \right)_+ - (1+x) \ln \frac{1-x}{x} + (1-x) \right] - \delta(1-x) (5 - \pi^2) C_F, \quad (46)$$

$$\overline{K}^{qg}(x) = \overline{K}^{\bar{q}g}(x) = P^{qg}(x) \ln \frac{1-x}{x} + C_F x, \quad (47)$$

$$\overline{K}^{gq}(x) = \overline{K}^{g\bar{q}}(x) = P^{gq}(x) \ln \frac{1-x}{x} + T_R 2x(1-x), \quad (48)$$

$$\begin{aligned} \overline{K}^{gg}(x) &= 2C_A \left[\left(\frac{1}{1-x} \ln \frac{1-x}{x} \right)_+ + \left(\frac{1-x}{x} - 1 + x(1-x) \right) \ln \frac{1-x}{x} \right] \\ &\quad - \delta(1-x) \left[\left(\frac{50}{9} - \pi^2 \right) C_A - \frac{16}{9} T_R N_f \right], \end{aligned} \quad (49)$$

$$\overline{K}^{\bar{q}q}(x) = \overline{K}^{q\bar{q}}(x) = 0, \quad (50)$$

and

$$\tilde{K}^{ab}(x) = P_{\text{reg}}^{ab}(x) \ln(1-x) + \delta^{ab} \mathbf{T}_a^2 \left[\left(\frac{2}{1-x} \ln(1-x) \right)_+ - \frac{\pi^2}{3} \delta(1-x) \right] \quad (51)$$

depend on the factorization scheme through the term $K_{\text{F.S.}}^{aa'}(x)$, which vanishes in the $\overline{\text{MS}}$ -scheme, and also on the regular parts of the Altarelli-Parisi splitting distributions given by $P_{\text{reg}}^{ab}(x) = P^{ab}(x)$, if $a \neq b$, and otherwise by

$$P_{\text{reg}}^{qq}(x) = -C_F(1+x) \quad \text{and} \quad P_{\text{reg}}^{gg}(x) = 2C_A \left[\frac{1-x}{x} - 1 + x(1-x) \right]. \quad (52)$$

The last line in Eq. (34) contains therefore the finite remainders that are left after the factorization of collinear initial-state singularities into the parton densities in the $\overline{\text{MS}}$ -scheme at the factorization scale μ_F . As guaranteed by the Kinoshita-Lee-Nauenberg and factorization theorems, the total NLO cross section is then not only UV-, but also IR-finite.

Finally, one subtlety must still be addressed: in Fig. 6, the center and right diagrams of lines one and three proceed through a squark propagator, which can become on-shell if $m_{\bar{q}} \geq m_{\tilde{\chi}}$ and $s \geq (m_{\bar{q}} + m_{\tilde{\chi}})^2$. To avoid double counting, the resonance contribution

$$d\sigma_{qg}^{(\bar{q})} = d\sigma(qg \rightarrow \tilde{\chi}\bar{q}) \text{BR}(\bar{q} \rightarrow \tilde{\chi}q) \quad (53)$$

must be subtracted from the gaugino pair production process using the narrow-width approximation, as it is identified experimentally as the associated production of a gaugino and a squark (Fig. 7), followed by the decay of the squark into a gaugino and a quark (Fig. 8).

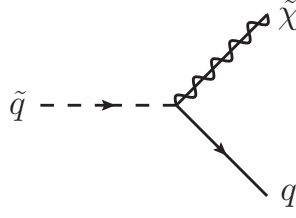


FIG. 8: Tree-level diagram for a squark decaying into a gaugino and a quark.

III. THRESHOLD RESUMMATION AT NEXT-TO-LEADING LOGARITHMIC ACCURACY

In the previous section, we have demonstrated that all soft and collinear (IR) singularities in the partonic NLO cross section $d\sigma_{ab}^{(1)}$ either cancel among virtual and real corrections or can be absorbed at the factorization scale μ_F into parton density functions (PDFs) $f_{a,b/A,B}(x_{a,b}, \mu_F^2)$, which represent probability distributions for initial partons a, b with longitudinal momentum fraction $x_{a,b}$ in the external hadrons A, B (e.g. protons or anti-protons). The QCD factorization theorem guarantees that the observable hadronic cross section

$$M^2 \frac{d\sigma_{AB}}{dM^2}(\tau) = \sum_{ab} \int_0^1 dx_a dx_b dz [x_a f_{a/A}(x_a, \mu^2)] [x_b f_{b/B}(x_b, \mu^2)] [z d\sigma_{ab}(z, M^2, \mu^2)] \delta(\tau - x_a x_b z) \quad (54)$$

can be obtained by convolving the process-dependent partonic cross section

$$d\sigma_{ab}(z, M^2, \mu^2) = \sum_{n=0}^{\infty} a_s^n(\mu^2) d\sigma_{ab}^{(n)}(z, M^2, \mu^2) \quad (55)$$

with universal PDFs. For the sake of simplicity, we will identify in the remainder of this paper the factorization scale μ_F and the renormalization scale μ_R , which enters the partonic cross section through the perturbative expansion in the (reduced) strong coupling constant $a_s(\mu_R^2) = \alpha_s(\mu_R^2)/(2\pi)$ and also explicitly beyond LO, with the common scale μ . M^2 represents the invariant mass squared of the (colorless) gaugino pair produced at LO, which carries the fractions $\tau = M^2/S$ and $z = M^2/s$ of the hadronic and partonic center-of-mass energies S and $s = x_a x_b S$, respectively. At LO, where no additional partons are produced besides the gaugino pair, the partonic cross section

$$d\sigma_{ab}^{(0)}(z, M^2, \mu^2) = \sigma_{ab}^{(0)}(M^2) \delta(1 - z) \quad (56)$$

is independent of μ and has its support entirely at the point $z = 1$. At higher order in QCD, the cancellation of soft and collinear parton emission among virtual and real corrections is restricted by the phase space boundary of the latter. This leads to logarithmic contributions $a_s^n [\ln^m(1-z)/(1-z)]_+$ with $m \leq 2n - 1$ (see Eqs. (40) and (45)), which become large close to the partonic threshold at $z \rightarrow 1$. Consequently, they spoil the convergence of the perturbative series and must be resummed to all orders in a_s .

By applying a Mellin transform

$$F(N) = \int_0^1 dy y^{N-1} F(y) \quad (57)$$

to the quantities $F = \sigma_{AB}$, σ_{ab} , and $f_{a,b/A,B}$ with $y = \tau$, z , and $x_{a,b}$ in Eq. (54), the hadronic cross section can be written as a simple product

$$M^2 \frac{d\sigma_{AB}}{dM^2}(N-1) = \sum_{ab} f_{a/A}(N, \mu^2) f_{b/B}(N, \mu^2) \sigma_{ab}(N, M^2, \mu^2), \quad (58)$$

the large logarithms in $z \rightarrow 1$ turn into large logarithms of the Mellin variable N ,

$$\left(\frac{\ln^m(1-z)}{1-z} \right)_+ \rightarrow \ln^{m+1} N \text{ etc.}, \quad (59)$$

and it is thus possible, in the $N \rightarrow \infty$ limit, to retain only the leading powers in N . In particular, one can neglect among the N -moments of the Altarelli-Parisi splitting functions at $\mathcal{O}(a_s)$

$$P^{qq}(N) = \gamma_{qq}^{(1)}(N) = C_F \left[\frac{3}{2} + \frac{1}{N(N+1)} - 2 \sum_{k=1}^N \frac{1}{k} \right] \rightarrow C_F \left(\frac{3}{2} - 2 \ln \bar{N} \right) + \mathcal{O} \left(\frac{1}{N} \right), \quad (60)$$

$$P^{qg}(N) = \gamma_{qg}^{(1)}(N) = C_F \left[\frac{2+N+N^2}{N(N^2-1)} \right] \rightarrow \frac{C_F}{N}, \quad (61)$$

$$P^{gq}(N) = \gamma_{gq}^{(1)}(N) = T_R \left[\frac{2+N+N^2}{N(N+1)(N+2)} \right] \rightarrow \frac{T_R}{N}, \text{ and} \quad (62)$$

$$P^{gg}(N) = \gamma_{gg}^{(1)}(N) = 2C_A \left[\frac{1}{N(N-1)} + \frac{1}{(N+1)(N+2)} - \sum_{k=1}^N \frac{1}{k} \right] + \beta_0 \rightarrow -2C_A \ln \bar{N} + \beta_0 + \mathcal{O} \left(\frac{1}{N} \right) \quad (63)$$

those which are not diagonal. Here, we have introduced the variable $\bar{N} = Ne^{\gamma_E}$, where γ_E is the Euler constant.

A. Refactorization

The resummation of the large logarithms in Eqs. (40) and (45) is based on the observation that the separation of the non-perturbative PDFs $f_{a,b/A,B}$ and the perturbative partonic cross section σ_{ab} in Eq. (58) is not unambiguously defined. It is in particular possible to re-factorize the partonic cross section [22]

$$\sigma_{ab}(N, M^2, \mu^2) = H_{ab}(M^2, \mu^2) \frac{\psi_{a/a}(N, M^2) \psi_{b/b}(N, M^2)}{f_{a/a}(N, \mu^2) f_{b/b}(N, \mu^2)} S_{ab}(N, M^2) + \mathcal{O} \left(\frac{1}{N} \right) \quad (64)$$

into a hard function H_{ab} , which is non-singular in and in fact independent of N , a ratio of PDFs in partons $\psi_{a,b}$ and $f_{a,b}$ defined at fixed *energy* and longitudinal momentum fraction, respectively, and a function S_{ab} , which describes the emission of soft gluons and can thus be computed in the eikonal approximation. The hard function

$$H_{ab}(M^2, \mu^2) = \sum_{n=0}^{\infty} a_s^n(\mu^2) H_{ab}^{(n)}(M^2, \mu^2) \quad (65)$$

can be expanded as a power series in a_s . Its LO and NLO coefficients read

$$H_{ab}^{(0)}(M^2, \mu^2) = \sigma_{ab}^{(0)}(M^2) \text{ and} \quad (66)$$

$$H_{ab}^{(1)}(M^2, \mu^2) = \sigma_{ab}^{(0)}(M^2) \left[\mathcal{A}_0 + \left(\gamma_a^{(1)} + \gamma_b^{(1)} \right) \ln \frac{M^2}{\mu^2} \right], \quad (67)$$

where \mathcal{A}_0 represents the IR-finite part of the renormalized virtual correction

$$\sigma_{ab}^{(V)}(M^2, \mu^2) = a_s \left(\frac{4\pi\mu^2}{M^2} \right)^\epsilon \frac{\Gamma(1-\epsilon)}{\Gamma(1-2\epsilon)} \left(\frac{\mathcal{A}_{-2}}{\epsilon^2} + \frac{\mathcal{A}_{-1}}{\epsilon} + \mathcal{A}_0 \right) \sigma_{ab}^{(0)}(M^2) + \mathcal{O}(\epsilon). \quad (68)$$

The PDFs satisfy the evolution equations [23]

$$\frac{\partial f_{c/a}(N, \mu^2)}{\partial \ln \mu^2} = \sum_b \gamma_{bc}(N, a_s(\mu^2)) f_{b/a}(N, \mu^2), \quad (69)$$

governed by the (gauge-independent) anomalous dimensions $\gamma_{aa'}(N, a_s(\mu^2)) = \sum_n a_s^n(\mu^2) \gamma_{aa'}^{(n)}(N)$ of the composite Wilson operators with $\gamma_{aa'}^{(1)}(N)$ given above, and [22]

$$\frac{\partial \psi_{a/a}(N, \mu^2)}{\partial \ln \mu^2} = \gamma_a(a_s(\mu^2)) \psi_{a/a}(N, \mu^2), \quad (70)$$

where the (gauge-dependent) anomalous dimensions $\gamma_a = 1/Z_a \partial Z_a / \partial \ln \mu^2 = \sum_n a_s^n(\mu^2) \gamma_a^{(n)}$ of the fields a correspond in the axial gauge [24] to the N -independent (virtual) parts of $\gamma_{aa}(N)$ [46]. In the singlet/non-singlet basis and to one-loop order, the evolution equations for $f_{c/a}$ can be solved and written in the closed exponential form [25]

$$f_{c/a}(N, \mu^2) = \sum_b E_{bc}(N, \mu^2, \mu_0^2) f_{b/a}(N, \mu_0^2), \quad (71)$$

where the evolution operator $E(N, \mu^2, \mu_0^2)$ satisfies the same evolution equation, Eq. (69), as $f_{c/a}(N, \mu^2)$. The ratio

$$\frac{\psi_{a/a}(N, M^2)}{f_{a/a}(N, \mu^2)} = \Delta_a(N, M^2, \mu^2) U_a(N, M^2)^{1/2} \quad (72)$$

has been shown [22] to exponentiate to all orders into a gauge-independent, but scheme- and scale-dependent function

$$\ln \Delta_a(N, M^2, \mu^2) = \int_0^1 dz \frac{z^{N-1} - 1}{1-z} \left[\int_{(1-z)^{m_s} \mu^2}^{(1-z)^2 M^2} \frac{dq^2}{q^2} A_a(a_s(q^2)) - B_a(a_s((1-z)^{m_s} M^2)) \right] \quad (73)$$

with $m_s = 0$ and consequently $B_a = 0$ in the $\overline{\text{MS}}$ -scheme, which describes the soft and *collinear* gluon radiation from the initial partons, and a gauge-dependent, but scheme- and scale independent function

$$\ln U_a(N, M^2) = - \int_0^1 dz \frac{z^{N-1} - 1}{1-z} \nu_a(a_s((1-z)^2 M^2)), \quad (74)$$

which can be combined with the soft function

$$\ln S_{ab}(N, M^2) = + \int_0^1 dz \frac{z^{N-1} - 1}{1-z} \lambda_a(a_s((1-z)^2 M^2)) \delta_{ab} \quad (75)$$

into the gauge-, scheme- and scale-independent function

$$\ln \Delta_{ab}(N, M^2) = \int_0^1 dz \frac{z^{N-1} - 1}{1-z} D_{ab}(a_s((1-z)^2 M^2)). \quad (76)$$

The functions U_a and S_{ab} can be computed in the eikonal approximation. They depend on the cusp anomalous dimension $\nu_a = 2C_a(\gamma \coth \gamma - 1)$ [26] of the considered process and describe soft *wide-angle* radiation.

B. NLL approximation

The coefficients

$$A_a(a_s) = \sum_{n=1}^{\infty} a_s^n A_a^{(n)}, \quad B_a(a_s) = \sum_{n=1}^{\infty} a_s^n B_a^{(n)}, \quad \text{and} \quad D_{ab}(a_s) = \sum_{n=1}^{\infty} a_s^n D_{ab}^{(n)} \quad (77)$$

can be expanded as power series in a_s , and the NLL results read [22, 27]

$$A_a^{(1)} = 2C_a, \quad (78)$$

$$A_a^{(2)} = 2C_a \left[\left(\frac{67}{18} - \frac{\pi^2}{6} \right) C_A - \frac{5}{9} N_f \right], \quad (79)$$

$$B_a^{(1)} = 0 \text{ (in the } \overline{\text{MS}} \text{ scheme), and} \quad (80)$$

$$D_{ab}^{(1)} = 0 \text{ (since } \nu_a^{(1)} = \lambda_a^{(1)}) \quad (81)$$

with $\nu_a^{(1)} = 4C_a$ and $C_a = C_F$ and C_A for an incoming quark ($a = q$) and gluon ($a = g$), respectively. Note, however, that $D_{ab}^{(2)} \neq 0$ [28]. After the integrations in Eqs. (73) and (76) have been performed, the partonic cross section in Eq. (64) can be written in the closed exponential form [28]

$$\sigma_{ab}(N, M^2, \mu^2) = \mathcal{H}_{ab}(M^2, \mu^2) \exp[\mathcal{G}_{ab}(N, M^2, \mu^2)] + \mathcal{O}\left(\frac{1}{N}\right). \quad (82)$$

Here, the perturbative coefficients of the hard function

$$\mathcal{H}_{ab}(M^2, \mu^2) = \sum_{n=0}^{\infty} a_s^n(\mu^2) \mathcal{H}_{ab}^{(n)}(M^2, \mu^2) \quad (83)$$

have been redefined with respect to those in Eq. (65) in order to absorb the non-logarithmic terms resulting from the integration, i.e.

$$\mathcal{H}_{ab}^{(0)}(M^2, \mu^2) = \sigma_{ab}^{(0)}(M^2) \text{ and} \quad (84)$$

$$\mathcal{H}_{ab}^{(1)}(M^2, \mu^2) = \sigma_{ab}^{(0)}(M^2) \left[\mathcal{A}_0 + \frac{\pi^2}{6} (A_a^{(1)} + A_b^{(1)}) + (\gamma_a^{(1)} + \gamma_b^{(1)}) \ln \frac{M^2}{\mu^2} \right]. \quad (85)$$

The coefficient function $\mathcal{H}_{ab}^{(1)}(M^2, \mu^2)$ given here agrees with the one presented in Eq. (115) of Ref. [17] except for their last three terms. While their last term corresponds to the flavor-diagonal collinear improvement to be discussed below, the two other terms represent leading and next-to-leading logarithms and should therefore not be present. Furthermore, the two terms in $(\ln 4\pi\mu_r^2/Q^2 - \gamma_E)$ should be squared individually, not together, and the virtual correction $\tilde{\mathcal{M}}_V^{\text{QCD}}$ defined in Eq. (116) of Ref. [17] should include the complete SUSY-QCD contributions and not only their UV-singular parts. The function \mathcal{G}_{ab} takes the form

$$\mathcal{G}_{ab}(N, M^2, \mu^2) = Lg_{ab}^{(1)}(\lambda) + g_{ab}^{(2)}(\lambda, M^2/\mu^2) + a_s g_{ab}^{(3)}(\lambda, M^2/\mu^2) + \dots \quad (86)$$

with $\lambda = a_s \beta_0 L$ and $L = \ln \bar{N}$. The first term in Eq. (86),

$$Lg_{ab}^{(1)}(\lambda) = \frac{L}{2\lambda\beta_0} (A_a^{(1)} + A_b^{(1)}) [2\lambda + (1-2\lambda) \ln(1-2\lambda)], \quad (87)$$

collects the leading logarithmic (LL) large- N contributions $L(a_s L)^n$ and depends on $A_{a,b}^{(1)}$ only. The coefficients $A_{a,b}^{(2)}$, $A_{a,b}^{(1)}$ and $D_{ab}^{(1)}$ determine the function

$$\begin{aligned} 2\beta_0 g_{ab}^{(2)}(\lambda, M^2/\mu^2) &= (A_a^{(1)} + A_b^{(1)}) \ln(1-2\lambda) \ln \frac{M^2}{\mu^2} \\ &+ (A_a^{(1)} + A_b^{(1)}) \frac{\beta_1}{\beta_0^2} [2\lambda + \ln(1-2\lambda) + \frac{1}{2} \ln^2(1-2\lambda)] \\ &- (A_a^{(2)} + A_b^{(2)}) \frac{1}{\beta_0} [2\lambda + \ln(1-2\lambda)] + D_{ab}^{(1)} \ln(1-2\lambda), \end{aligned} \quad (88)$$

which resums the next-to-leading logarithmic (NLL) terms $(a_s L)^n$. Similarly, the functions $g_{ab}^{(n+1)}$ resum the N^n LL terms and depend on the coefficients $A_{a,b}^{(n+1)}$, $A_{a,b}^{(k)}$ and $D_{ab}^{(k)}$ with $1 \leq k \leq n$.

C. Collinear improvement

Up to this point, we have systematically neglected all terms of $\mathcal{O}(1/N)$. However, since the dominant $1/N$ -terms, i.e. those of the form $a_s^n L^{2n-1}/N$, stem from the universal collinear radiation of initial state partons, they are expected to exponentiate as well. This has been proven to next-to-next-to-leading order for deep-inelastic scattering and Drell-Yan type processes [29] and can be achieved by making the replacement (cf. Eq. (97) below)

$$\mathcal{H}_{ab}^{(1)} \rightarrow \mathcal{H}_{ab}^{(1)} + L \frac{A_a^{(1)} + A_b^{(1)}}{N} \mathcal{H}_{ab}^{(0)}, \quad (89)$$

i.e. by including the corresponding subleading terms of the *diagonal* splitting functions $\gamma_{aa,bb}(N)$ in Eqs. (60) and (63). Carrying on with this argument, it is even possible to resum the terms of $\mathcal{O}(1/N)$ coming from the diagonal and non-diagonal splitting functions by identifying the terms [30]

$$Lg_{ab}^{(1)}(\lambda) = \frac{L}{2\lambda\beta_0} (A_a^{(1)} + A_b^{(1)}) [(-2\lambda) \ln(1-2\lambda)] + \dots \quad (90)$$

with the LL approximation of the QCD evolution operators E_{ab} defined in Eq. (71) and then promoting the LL to the full one-loop approximation $E_{ab}^{(1)}$. The resummed cross section, Eq. (82), can then be written in a collinearly improved form as

$$\sigma_{ab}(N, M^2, \mu^2) = \sum_{a',b'} E_{aa'}^{(1)}(N, M^2/\bar{N}^2, \mu_F^2) \tilde{\mathcal{H}}_{a'b'}(M^2, \mu_R^2) \exp[\tilde{\mathcal{G}}_{a'b'}(N, M^2, \mu_R^2)] E_{bb'}^{(1)}(N, M^2/\bar{N}^2, \mu_F^2), \quad (91)$$

where the dependences on the factorization and renormalization scales have been recovered explicitly, the collinearly improved hard coefficient function $\tilde{\mathcal{H}}_{ab}$ is expanded as usual as a power series in $a_s(\mu^2)$ and its LO and NLO coefficients read now

$$\tilde{\mathcal{H}}_{ab}^{(0)}(M^2, \mu^2) = \sigma_{ab}^{(0)}(M^2) \text{ and} \quad (92)$$

$$\tilde{\mathcal{H}}_{ab}^{(1)}(M^2, \mu^2) = \sigma_{ab}^{(0)}(M^2) \left[\mathcal{A}_0 + \frac{\pi^2}{6} (A_a^{(1)} + A_b^{(1)}) \right], \quad (93)$$

and the Sudakov exponential function $\tilde{\mathcal{G}}_{ab}$ is expanded in the same way as \mathcal{G}_{ab} in Eq. (86) with

$$\begin{aligned} L\tilde{g}_{ab}^{(1)}(\lambda) &= \frac{L}{2\lambda\beta_0}(A_a^{(1)} + A_b^{(1)})[2\lambda + \ln(1 - 2\lambda)] \text{ and} \quad (94) \\ 2\beta_0\tilde{g}_{ab}^{(2)}(\lambda, M^2/\mu^2) &= (A_a^{(1)} + A_b^{(1)})[2\lambda + \ln(1 - 2\lambda)] \ln \frac{M^2}{\mu^2} \\ &+ (A_a^{(1)} + A_b^{(1)}) \frac{\beta_1}{\beta_0^2} [2\lambda + \ln(1 - 2\lambda) + \frac{1}{2} \ln^2(1 - 2\lambda)] \\ &- (A_a^{(2)} + A_b^{(2)}) \frac{1}{\beta_0} [2\lambda + \ln(1 - 2\lambda)] \\ &+ (-2\gamma_a^{(1)} - 2\gamma_b^{(1)} + D_{ab}^{(1)}) \ln(1 - 2\lambda). \quad (95) \end{aligned}$$

Here, the anomalous dimensions $\gamma_{a,b}^{(1)}$ in $\tilde{g}_{ab}^{(2)}(\lambda, M^2/\mu^2)$ have been introduced to cancel the NLL terms in the one-loop approximation $E_{ab}^{(1)}$ of the evolution operators.

For the Drell-Yan process, it has been suggested that also the constant terms in the hard coefficient function $\tilde{\mathcal{H}}_{ab}^{(1)}(M^2, \mu^2)$ can be exponentiated, since these terms factorize the complete Born cross section, include finite remainders of the infrared singularities in the virtual corrections and are thus related to the corresponding singularities in the real corrections giving rise to the large logarithms [31]. While this choice is supported by an explicit two-loop calculation [32] and can be applied to other Drell-Yan like processes [14], gaugino pair production does not proceed through a single s -channel diagram, and the virtual corrections thus factorize only at the level of amplitudes, but not the full cross section. Resumming some or all of the finite terms in the hard coefficient function $\tilde{\mathcal{H}}_{ab}^{(1)}(M^2, \mu^2)$ into an exponential as in Ref. [17] seems therefore not to be justified in this case.

D. Matching and inverse Mellin transform

As mentioned above, the large logarithms, which spoil the convergence of the perturbative series and must be resummed to all orders, appear close to production threshold. Conversely, the perturbative cross section should be valid far from this threshold. To obtain a reliable prediction in all kinematic regions, both results must be consistently matched through

$$\sigma_{ab} = \sigma_{ab}^{(\text{res.})} + \sigma_{ab}^{(\text{f.o.})} - \sigma_{ab}^{(\text{exp.})}, \quad (96)$$

i.e. by subtracting from the sum of the resummed (res.) cross section in Eq. (91) and the fixed order (f.o.) cross section in Eq. (34) their overlap. The latter can be obtained by expanding (exp.) the resummed cross section to the same fixed order as the perturbative result. At $\mathcal{O}(a_s)$, one then obtains

$$\begin{aligned} \sigma_{ab}^{(\text{exp.})}(N, M^2, \mu^2) &= \tilde{\mathcal{H}}_{ab}^{(0)}(M^2, \mu^2) + a_s \tilde{\mathcal{H}}_{ab}^{(1)}(M^2, \mu^2) \\ &- a_s \left(2L - \ln \frac{M^2}{\mu^2} \right) \sum_c [\gamma_{ac}^{(1)}(N) \tilde{\mathcal{H}}_{cb}^{(0)}(M^2, \mu^2) + \tilde{\mathcal{H}}_{ac}^{(0)}(M^2, \mu^2) \gamma_{bc}^{(1)}(N)] \\ &- a_s \tilde{\mathcal{H}}_{ab}^{(0)}(M^2, \mu^2) [L^2(A_a^{(1)} + A_b^{(1)}) - 2L(\gamma_a^{(1)} + \gamma_b^{(1)})]. \quad (97) \end{aligned}$$

After the resummed result and its perturbative expansion have been obtained in Mellin N -space and multiplied with the N -moments of the PDFs according to Eq. (58), an inverse Mellin transform

$$M^2 \frac{d\sigma_{AB}}{dM^2}(\tau) = \frac{1}{2\pi i} \int_{\mathcal{C}_N} dN \tau^{-N} M^2 \frac{d\sigma_{AB}(N)}{dM^2} \quad (98)$$

must be performed in order to obtain the observed hadronic cross section as a function of $\tau = M^2/S$. Special attention must be paid to the singularities in the resummed exponents $\tilde{g}_{ab}^{(1,2)}$, which are situated at $\lambda = 1/2$ and are related to the Landau pole of the perturbative coupling a_s . To avoid this pole as well as those in the Mellin moments of the PDFs related to the small- x (Regge) singularity $f_{a/A}(x, \mu_0^2) \propto x^\alpha(1-x)^\beta$ with $\alpha < 0$, we choose an integration contour \mathcal{C}_N according to the *principal value* procedure proposed in Ref. [33] and the *minimal prescription* proposed in Ref. [34] and define two branches

$$\mathcal{C}_N : N = C + ze^{\pm i\phi} \quad \text{with } z \in [0, \infty[, \quad (99)$$

where the constant C is chosen such that the singularities of the N -moments of the PDFs lie to the left and the Landau pole to the right of the integration contour. While formally the angle ϕ can be chosen in the range $[\pi/2, \pi[$, the integral converges faster, if $\phi > \pi/2$.

IV. NUMERICAL RESULTS

We now turn to our numerical analysis of threshold resummation effects on the production of various gaugino pairs at the Tevatron $p\bar{p}$ -collider ($\sqrt{S} = 1.96$ TeV) and the LHC pp -collider ($\sqrt{S} = 7 - 14$ TeV). For the masses and widths of the electroweak gauge bosons, we use the current values of $m_Z = 91.1876$ GeV and $m_W = 80.403$ GeV. The squared sine of the electroweak mixing angle

$$\sin^2 \theta_W = 1 - \frac{m_W^2}{m_Z^2} \quad (100)$$

and the electromagnetic fine structure constant

$$\alpha = \frac{\sqrt{2}G_F m_W^2 \sin^2 \theta_W}{\pi} \quad (101)$$

can be calculated in the improved Born approximation using the world average value of $G_F = 1.16637 \cdot 10^{-5}$ GeV⁻² for Fermi's coupling constant [35]. The CKM-matrix is assumed to be diagonal, and the top quark mass is taken to be 173.1 GeV [36]. The strong coupling constant is evaluated in the one-loop and two-loop approximation for LO and NLO/NLL+NLO results, respectively, with a value of $\Lambda_{\overline{\text{MS}}}^{n_f=5}$ corresponding to the employed LO (CTEQ6.6L1) and NLO (CTEQ6.6M) parton densities [37]. For the resummed and expanded contributions, the latter have been transformed numerically to Mellin N -space. When we present spectra in the invariant mass M of the gaugino pair, we identify the unphysical scales $\mu_F = \mu_R = \mu$ with M , whereas for total cross sections we identify them with the average mass of the two produced gauginos. The remaining theoretical uncertainty is estimated by varying the common scale μ about these central values by a factor of two up and down and the parton densities along the 22 eigenvector directions defined by the CTEQ collaboration.

A. Benchmark points

The running electroweak couplings as well as the physical masses of the SUSY particles and their mixing angles are computed with the computer program SPheno 2.2.3 [38], which includes a consistent calculation of the Higgs boson masses and all one-loop and the dominant two-loop radiative corrections in the renormalization group equations linking the restricted set of SUSY-breaking parameters at the gauge coupling unification scale to the complete set of observable SUSY masses and mixing angles at the electroweak scale. We choose the widely used minimal supergravity (mSUGRA) point SPS1a' [20] as the benchmark for most of our numerical studies. This point has an intermediate value of $\tan \beta = 10$ and $\mu > 0$ (favored by the rare decay $b \rightarrow s\gamma$ and the measured anomalous magnetic moment of the muon), a light gaugino mass parameter of $m_{1/2} = 250$ GeV, and a slightly lower scalar mass parameter $m_0 = 70$ GeV and trilinear coupling $A_0 = -300$ GeV than the original point SPS1a [39] in order to render it compatible with low-energy precision data, high-energy mass bounds, and the observed cold dark matter relic density. It is also similar to the post-WMAP point B' ($m_0 = 60$ GeV and $A_0 = 0$) [40], which has been adopted by the CMS collaboration as their first low-mass point (LM1) [41]. In the SPS1a' scenario, the $\tilde{\chi}_1^0$ is the LSP with a mass of 98 GeV, the gauginos producing the trilepton signal have masses of $m_{\tilde{\chi}_1^\pm} \simeq m_{\tilde{\chi}_2^0} = 184$ GeV, and the heavier gauginos, which decay mostly into the lighter gauginos, W and Z bosons as well as the lightest Higgs boson, have masses of $m_{\tilde{\chi}_3^0} = 400$ GeV and $m_{\tilde{\chi}_2^\pm} \simeq m_{\tilde{\chi}_4^0} = 415$ GeV. The average squark and gluino masses are $m_{\tilde{q}} \simeq 550$ GeV and $m_{\tilde{g}} = 604$ GeV.

TABLE II: Names, mSUGRA parameters, and physical SUSY particle masses of the benchmark points used in our numerical studies.

Scenario	m_0 [GeV]	$m_{1/2}$ [GeV]	A_0 [GeV]	$\tan\beta$	$\text{sgn}(\mu)$	$m_{\tilde{\chi}_1^0}$ [GeV]	$m_{\tilde{\chi}_1^\pm, \tilde{\chi}_2^0}$ [GeV]	$m_{\tilde{\chi}_3^0}$ [GeV]	$m_{\tilde{\chi}_2^\pm, \tilde{\chi}_4^0}$ [GeV]	$m_{\tilde{q}}$ [GeV]	$m_{\tilde{g}}$ [GeV]
SPS 1a'	70	250	-300	10	+	98	184	400	415	550	604
LM1	60	250	0	10	+	96	178	346	366	550	603
LM7	3000	230	0	10	+	94	176	337	359	3000	636
LM9	1450	175	0	50	+	70	128	263	284	1480	487
SU2	3550	300	0	10	+	124	229	355	384	3560	809
SU3	100	300	-300	6	+	118	223	465	481	650	715

Apart from the low-mass point LM1, we will also study the points LM7 and LM9, since all three points have been found by the CMS collaboration to lead to visible three-lepton signals. For LM7, the direct $\tilde{\chi}_1^\pm \tilde{\chi}_2^0$ production cross section exceeds even 70% of the total SUSY particle production cross section [41]. The ATLAS collaboration have studied the direct production of gauginos at the points SU2 and SU3 with or without a jet veto (denoted JV, i.e. no jet in the event with transverse momentum $p_T > 20$ GeV) in order to suppress the background from top quark pair production [42]. A summary of all scenarios considered here is presented in Tab. II. Note that none of these points falls into (but most of them lie relatively close to) the regions excluded by the Tevatron collaborations CDF and D0, which assume, however, a lower value of $\tan\beta = 3$ and always $A_0 = 0$ [16]. In Ref. [17], the cross section for the associated production of $\tilde{\chi}_1^\pm$ and $\tilde{\chi}_2^0$ has been computed as a function of $\tan\beta$ and $m_{1/2}$ for $m_0 = 200$ and 1000 GeV and assuming $A_0 = 0$ and $\mu > 0$. Unfortunately, the exact version of the renormalization group program SPheno used there could not be determined, and we were not able to reproduce the physical SUSY particle mass spectra of Ref. [17]. Since we also do not completely agree analytically with the coefficient function $\mathcal{H}_{ab}^{(1)}(M^2, \mu^2)$ of Ref. [17] (see above), we must refrain from a direct comparison of our numerical results.

B. Invariant mass spectra

In Fig. 9 we present invariant mass spectra $M^3 d\sigma/dM$ for the production of various combinations of $\tilde{\chi}_1^\pm$ and $\tilde{\chi}_2^0$ with $m_{\tilde{\chi}_1^\pm} \simeq m_{\tilde{\chi}_2^0} = 184$ GeV in the SPS1a' scenario at the Tevatron. The spectra start at $M = m_{\tilde{\chi}_1^\pm} + m_{\tilde{\chi}_2^0} = 368$ GeV and increase considerably from LO (blue) to NLO (grey), but much less from NLO to NLL+NLO (red). The scale uncertainty is considerably reduced from NLO to NLL+NLO, which indicates good convergence of the reorganized perturbative series. The cross section is smallest for the production of two neutralinos, since they are gaugino-like and couple only weakly to the s -channel Z -boson (see Tab. I). Since the Tevatron is a $p\bar{p}$ collider, the cross sections are identical for $\tilde{\chi}_2^0 \tilde{\chi}_1^-$ and $\tilde{\chi}_1^+ \tilde{\chi}_2^0$ (not shown) pairs. The largest cross section is obtained for chargino pairs due to the s -channel photon contribution. Threshold resummation should be most important as $M \rightarrow \sqrt{s}$ and $z \rightarrow 1$, but its effects on the partonic cross section are, of course, reduced in the hadronic cross section shown here by the parton densities, which tend to 0 as $x_{a,b}$ and $z \rightarrow 1$. Nevertheless, on close inspection one observes that the NLL+NLO cross section for two neutralinos no longer overlaps with the one at NLO for relatively large invariant masses of $M \simeq \sqrt{S}/2$.

A similar hierarchy of the different production channels is observed in Fig. 10 for the LHC with its current center-of-mass energy of $\sqrt{S} = 7$ TeV and in Fig. 11 for the LHC with its design energy of $\sqrt{S} = 14$ TeV. There are, however, two notable differences. First, the LHC is a pp collider, so that the cross section for $\tilde{\chi}_1^+ \tilde{\chi}_2^0$ exceeds the one for $\tilde{\chi}_1^- \tilde{\chi}_2^0$ by a factor of two and becomes even larger than the one for chargino pairs. Second, the NLO band is separated by a wider gap from the LO band than it was the case at Tevatron, whereas the NLL+NLO and NLO bands overlap considerably more. This is, of course, due to the fact that the light gauginos are now produced further away from the threshold of the 7 or 14 TeV collider, so that the importance of soft-gluon resummation is reduced. However, one still observes a sizeable reduction of the scale uncertainty from NLO to NLL+NLO.

Heavier gaugino pairs can only be produced with sizeable cross sections at the LHC. We therefore show in Figs. 12 and 13 the invariant mass spectra $M^3 d\sigma/dM$ for the production of various combinations of $\tilde{\chi}_{3,4}^0$ and $\tilde{\chi}_2^\pm$ at the LHC with $\sqrt{S} = 7$ TeV and 14 TeV and with $m_{\tilde{\chi}_3^0} = 400$ GeV and $m_{\tilde{\chi}_2^\pm} \simeq m_{\tilde{\chi}_1^0} = 415$ GeV in the SPS1a' scenario. The spectra start at $M \simeq 800 - 830$ GeV, and their magnitudes are considerably smaller than in the light gaugino case. However, they are now of comparable size for neutralino and chargino pairs due to the fact that the dominantly higgsino $\tilde{\chi}_3^0$ and $\tilde{\chi}_4^0$ now have sizeable couplings to the s -channel Z -boson (see Tab. I). The associated production of a neutralino and a chargino is again much larger for the positive chargino eigenstate than for its negative counterpart. The cross sections for $\tilde{\chi}_3^0 \tilde{\chi}_2^\pm$ pairs are very similar to those for $\tilde{\chi}_4^0 \tilde{\chi}_2^\pm$ pairs and therefore not shown. Higgsino-like

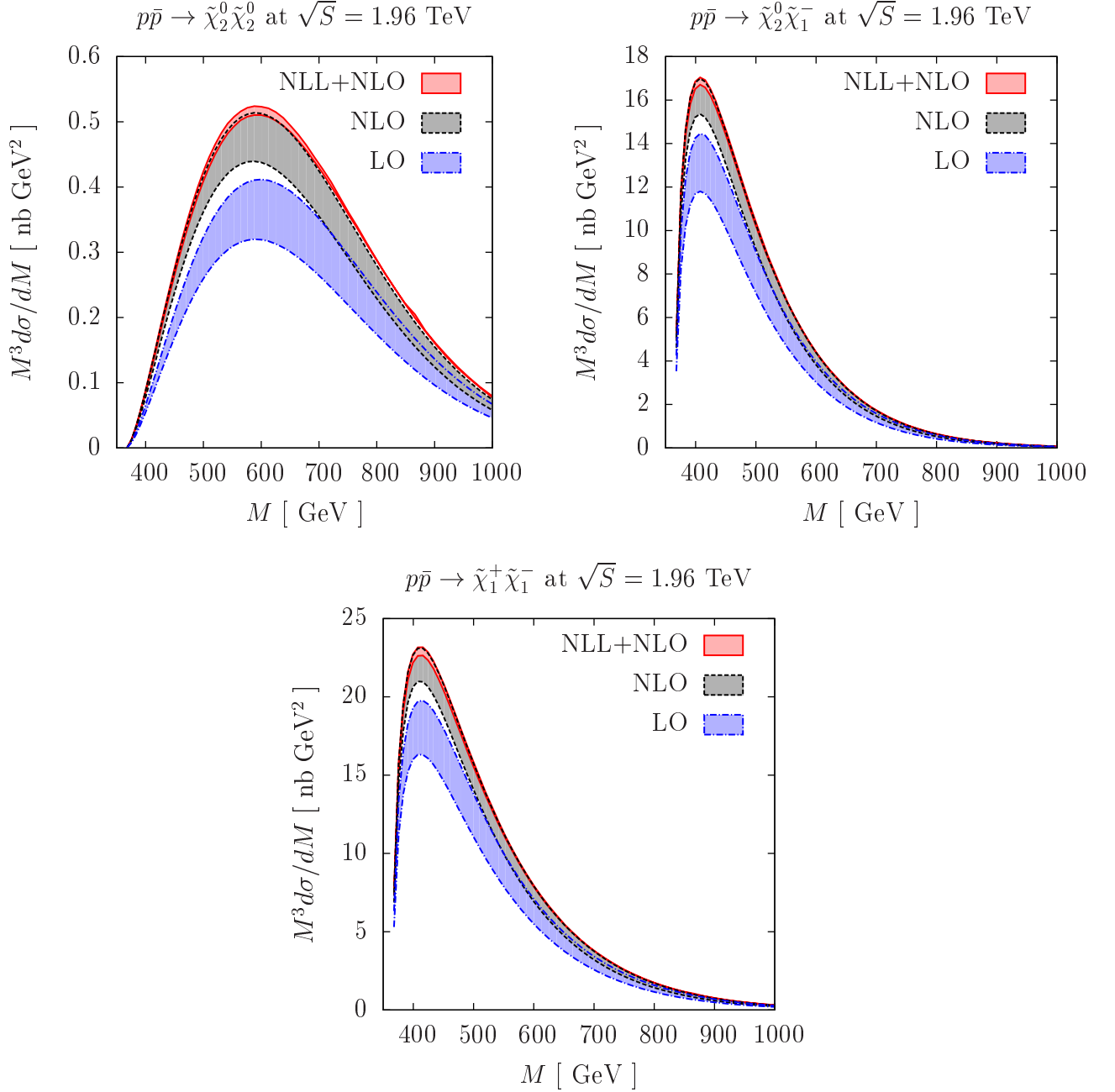


FIG. 9: Invariant mass spectra for the production of various light gaugino pairs at the Tevatron in the SPS1a' scenario and in the LO (blue), NLO (grey) and NLL+NLO (red) approximation. The corresponding scale uncertainties are represented by the band widths.

neutralinos and charginos with large s -channel contributions are produced as S -waves, so that the invariant mass spectra rise more steeply at low M than P -wave produced gaugino-like neutralinos and charginos.

From Figs. 9-13, the impact of threshold resummation effects is difficult to estimate. We therefore present in Fig. 14 the relative size

$$K^{\text{NLL}} = \frac{d\sigma^{\text{NLL+NLO}}}{d\sigma^{\text{NLO}}} \quad (102)$$

of the NLL+NLO prediction with respect to the NLO prediction. As one expects, the correction is larger at the Tevatron with its lower center-of-mass energy (top left) than at the LHC (top right and bottom) and increases with

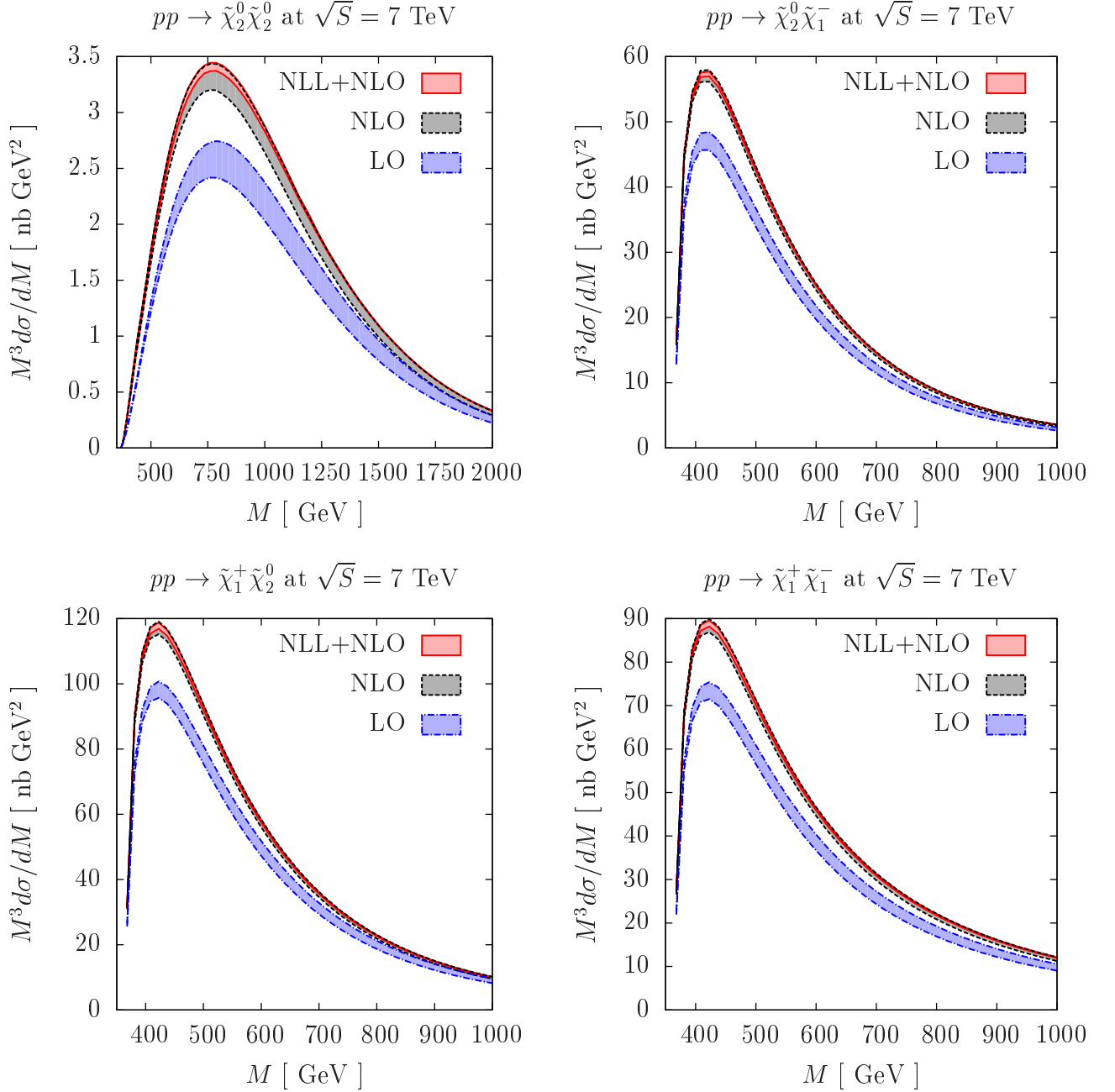


FIG. 10: Same as Fig. 9 for the LHC with its current center-of-mass energy of $\sqrt{S} = 7$ TeV.

the invariant mass. The relatively small differences among the K^{NLL} -factors for neutralino pair production and the channels involving at least one chargino can be traced to the fact that the former receives most of its contributions from t - and u -channel squark exchanges, which are more sensible to strong corrections than the exchanges of electroweak bosons in the s -channel.

The K^{NLL} -factors for the production of heavy gaugino pairs at the LHC with $\sqrt{S} = 7$ TeV (14 TeV) are presented in Fig. 15 left (right). They are larger than their counterparts for light gauginos in Fig. 14, since the gaugino masses as well as the invariant masses M are now closer to the hadronic center-of-mass energies. In addition, the result for the $\tilde{\chi}_3^0\tilde{\chi}_4^0$ channel differs no longer substantially from the other channels, since the heavy neutralinos are now higgsino-like and their production is now also dominated by the s -channel exchange of a weak gaugino.

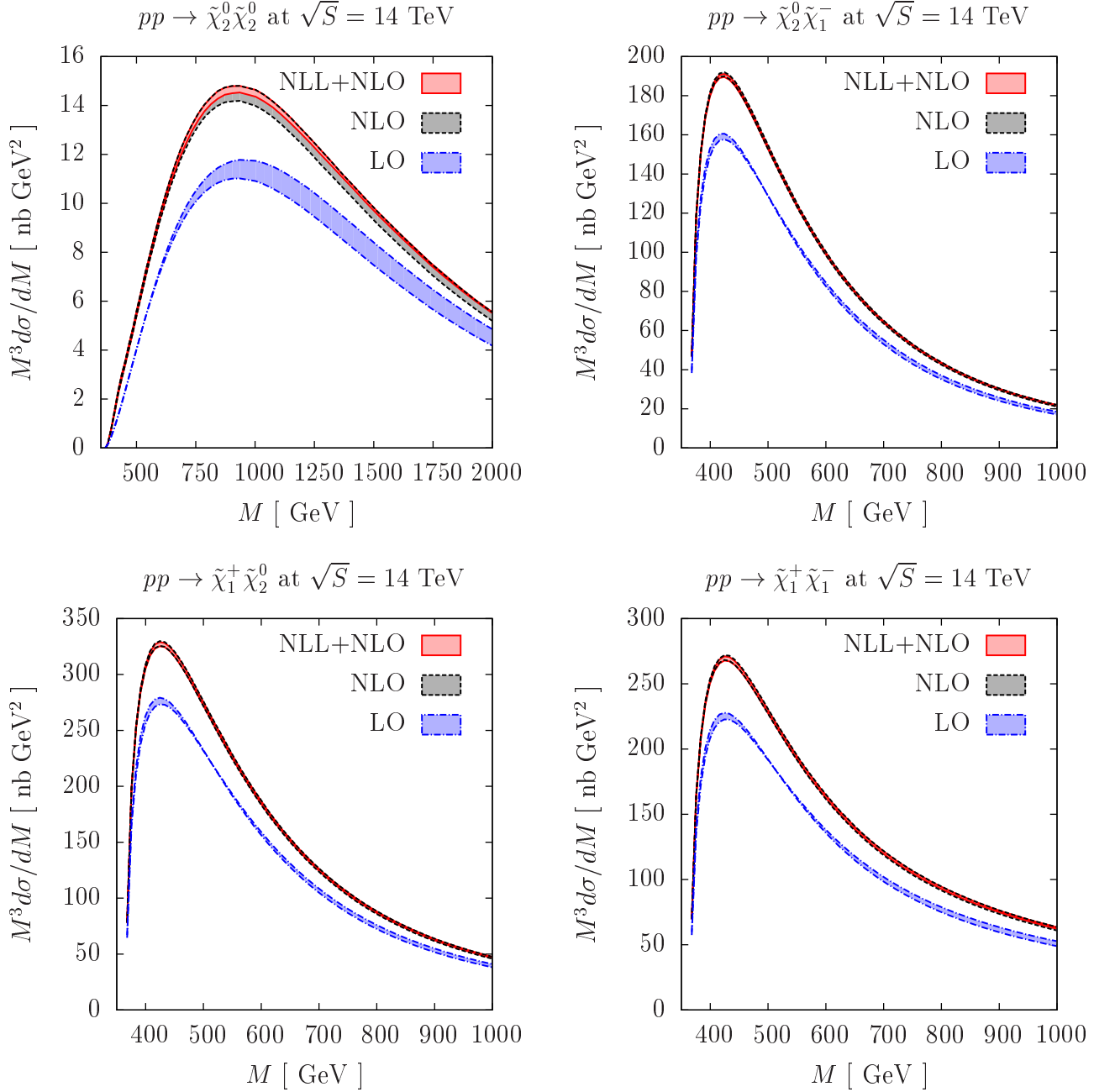


FIG. 11: Same as Fig. 9 for the LHC with its design center-of-mass energy of $\sqrt{S} = 14$ TeV.

C. Total cross sections

The stability of the perturbative series and its reorganization is traditionally checked by varying the factorization and renormalization scales μ_F and μ_R about a central value μ_0 . We therefore present now the total cross sections for the production of light gaugino pairs at the Tevatron (Fig. 16) and at the LHC with $\sqrt{S} = 7$ TeV (Fig. 17) as a function of the ratio $\mu_{F,R}/\mu_0$, where the central scale μ_0 is now chosen to be the average mass of the produced gaugino pair. The LO prediction (blue, dot-dashed) of the electroweak processes under consideration is, of course, independent of the renormalization scale μ_R (right part of the figures), whereas the NLO prediction (black, dashed) depends inversely on the logarithm of μ_R through the strong coupling $\alpha_s(\mu_R)$. At NLL accuracy (red, full), the resummed soft corrections attenuate this dependence and introduce a plateau region, so that the prediction is stabilized. The

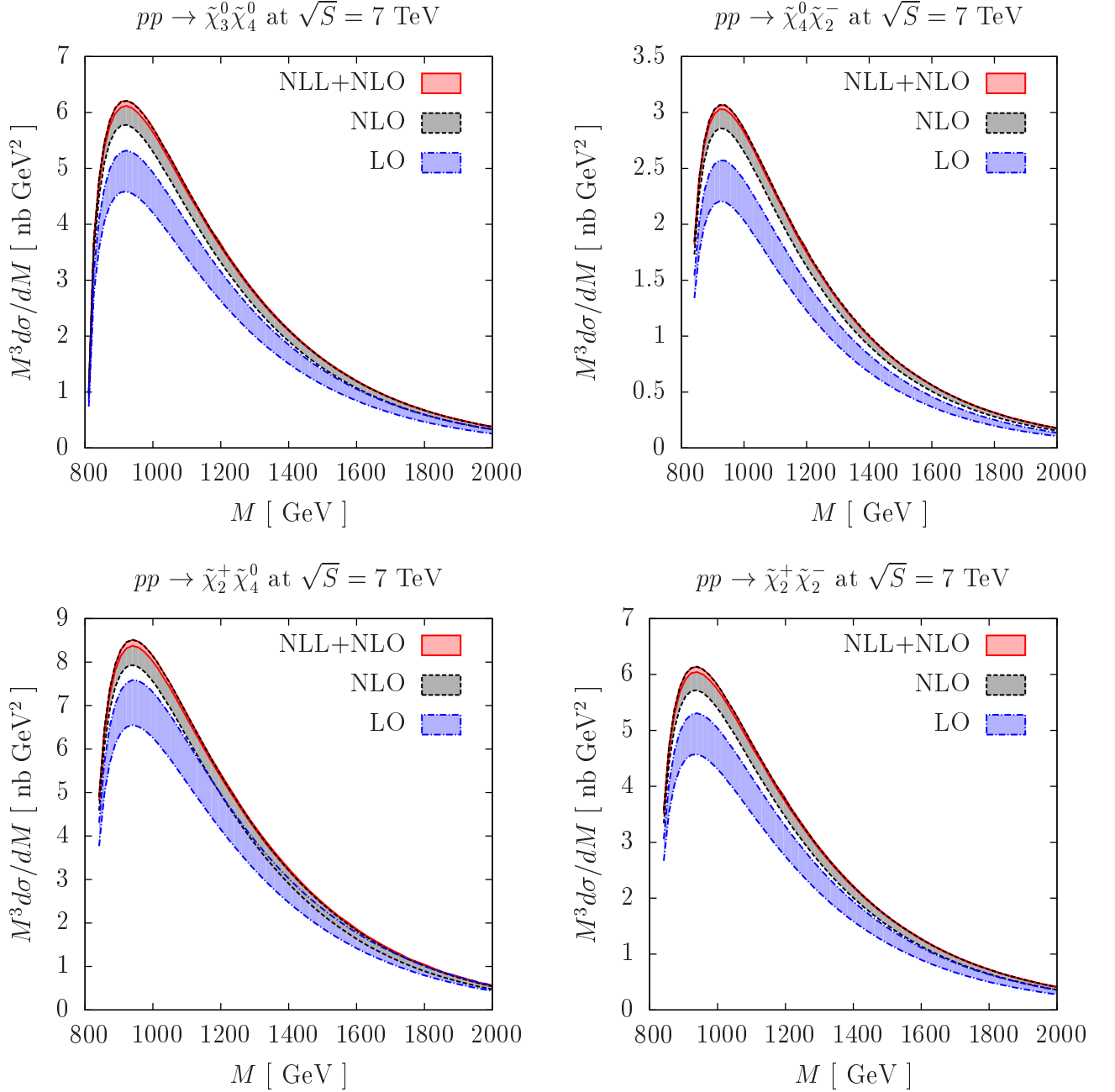


FIG. 12: Same as Fig. 9 for the production of heavy gaugino pairs at the LHC with its current center-of-mass energy of $\sqrt{S} = 7$ TeV.

factorization scale μ_F (central part of the figures) enters the hadronic cross section already at LO through the largely logarithmic dependence of the PDFs, which is then attenuated by the factorization of initial-state singularities at NLO and further at NLL accuracy. In all cases, the resulting total NLL+NLO prediction is thus much less dependent on the common scale $\mu_F = \mu_R = \mu$ (left part of the figures) than the LO and NLO estimates.

In Tab. III we present the total cross sections for the trilepton channel in the SPS1a' scenario at the Tevatron ($\sqrt{S} = 1.96$ TeV) and LHC ($\sqrt{S} = 7, 10$ and 14 TeV). Besides the central values (in fb) at LO, NLO and NLL+NLO, we also present the scale and PDF uncertainties. The former are estimated as described above by a common variation of the renormalization and factorization scales by a factor of two about the average mass of the two gauginos, the

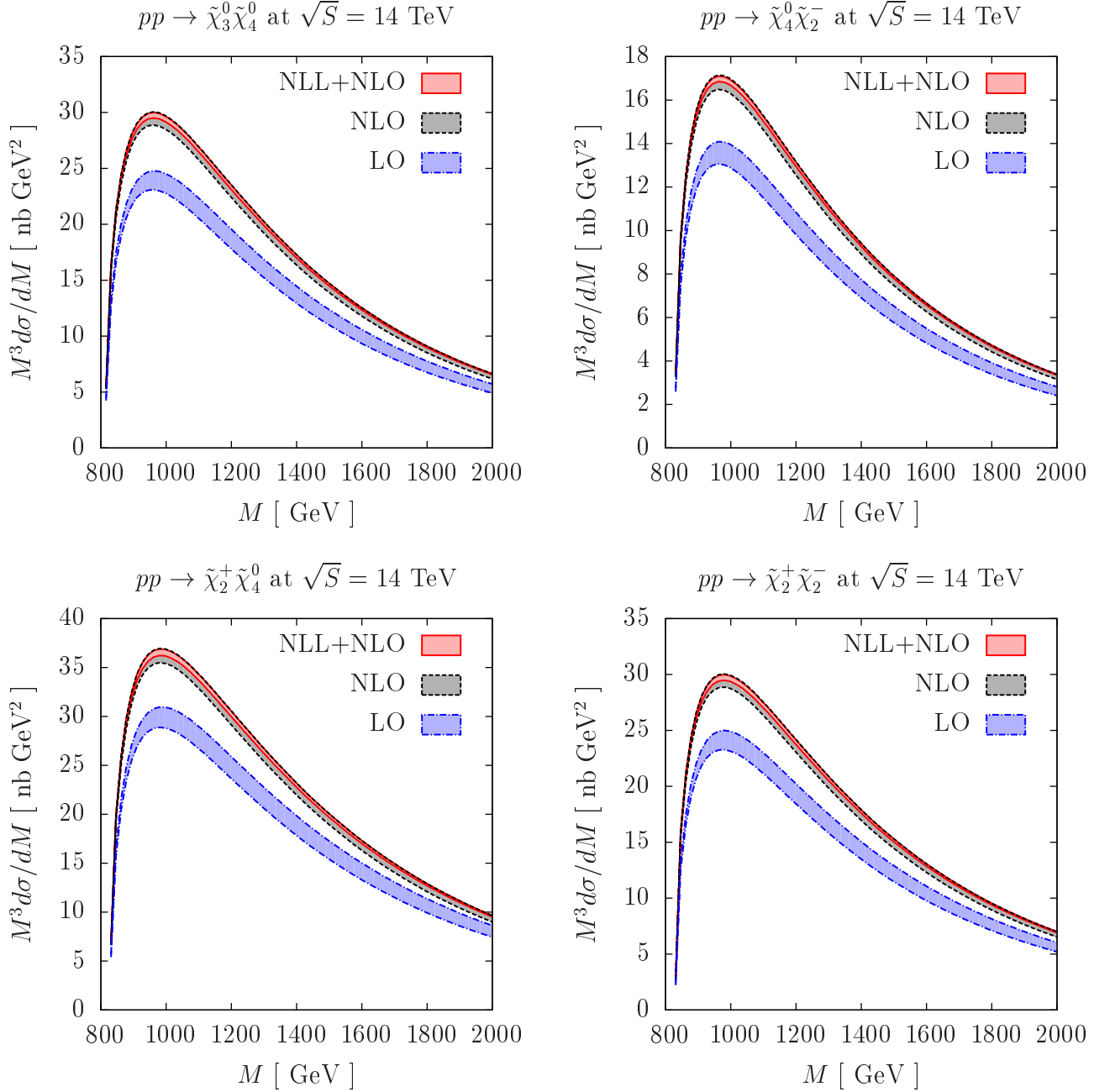


FIG. 13: Same as Fig. 9 for the production of heavy gaugino pairs at the LHC with its design center-of-mass energy of $\sqrt{S} = 14$ TeV.

latter through

$$\Delta\sigma_{\text{PDF}+} = \sqrt{\sum_{i=1}^{22} [\max(\sigma_{+i} - \sigma_0, \sigma_{-i} - \sigma_0, 0)]^2}, \quad \Delta\sigma_{\text{PDF}-} = \sqrt{\sum_{i=1}^{22} [\max(\sigma_0 - \sigma_{+i}, \sigma_0 - \sigma_{-i}, 0)]^2} \quad (103)$$

along the 22 eigenvector directions defined by the CTEQ collaboration. Since these are available only for the NLO fit CTEQ6.6M, but not for the LO fit CTEQ6.6L1, we do not present a PDF uncertainty for the LO prediction. Furthermore, the same PDF set enters at NLO and NLL+NLO, so that the PDF uncertainties for these two predictions coincide. The most important result is again the considerable reduction of the scale uncertainty from LO to NLO and then to NLL+NLO. The total cross sections increase with the available center-of-mass energy due to the higher

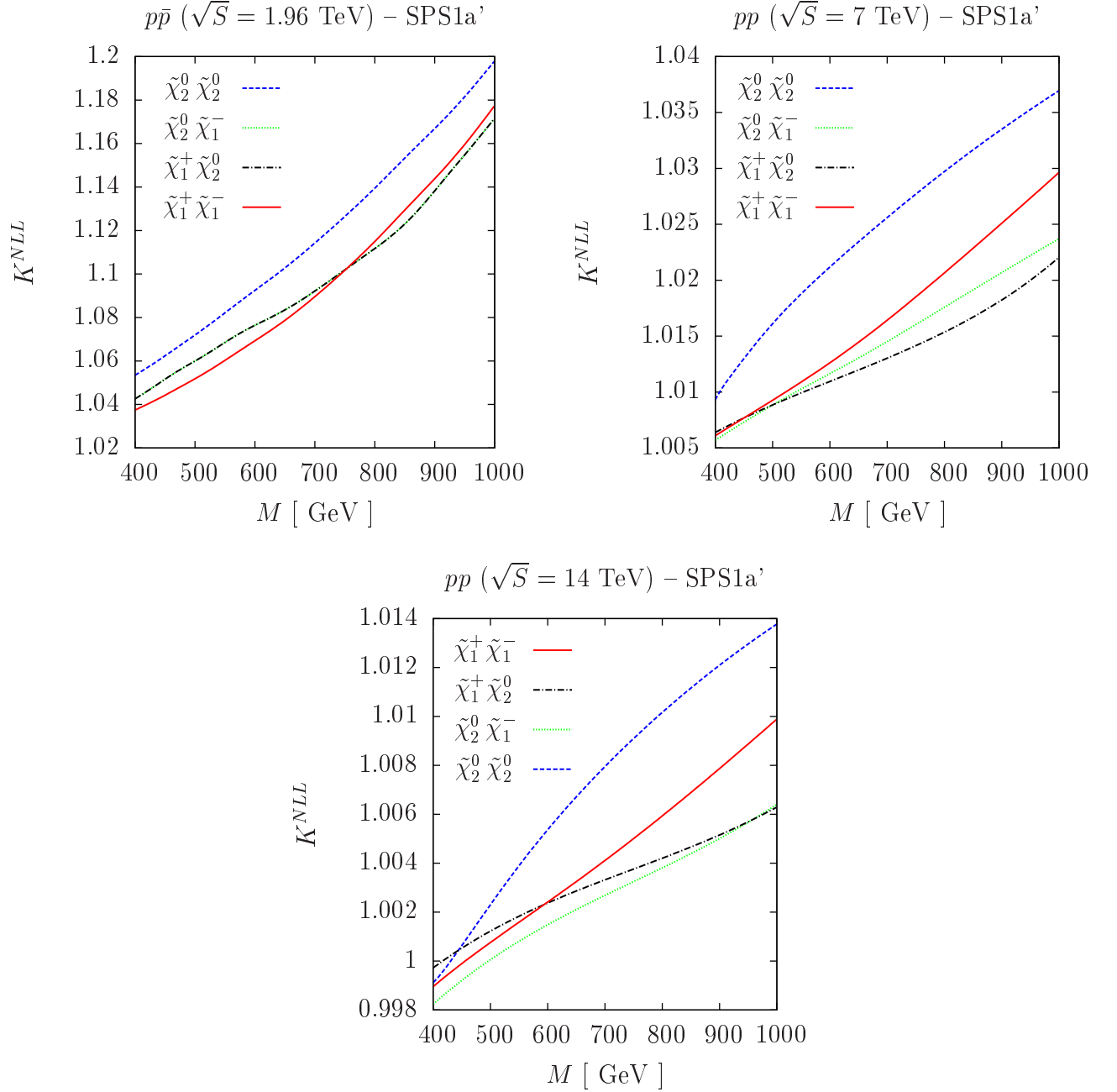


FIG. 14: Ratios K^{NLL} of NLL+NLO over NLO differential cross sections as a function of the invariant mass M of a light gaugino pair at the Tevatron (top left) and LHC with $\sqrt{S} = 7$ TeV (top right) and $\sqrt{S} = 14$ TeV (bottom) in the SPS1a' scenario.

parton luminosity at smaller values of x . A crude estimate gives

$$\sigma_{pp} = \int_{m^2/S}^1 d\tau f_{q/p}(x_q) f_{\bar{q}/p}(x_{\bar{q}}) \sigma_{q\bar{q}} \sim \int_{m^2/S}^1 d\tau \tau^{-1.8} \frac{1}{\tau S}, \sim \sqrt{S}^{1.6} \quad (104)$$

which agrees with the cross sections given in Tab. III surprisingly well.

In Tab. IV we fix the LHC center-of-mass energy to its design value of $\sqrt{S} = 14$ TeV and show the total production cross sections for light and heavy gaugino pairs in LO, NLO and NLL+NLO together with the corresponding theoretical uncertainties. As it was already mentioned above, the cross section for the higgsino-like $\tilde{\chi}_3^0 \tilde{\chi}_4^0$ pairs is about as large as

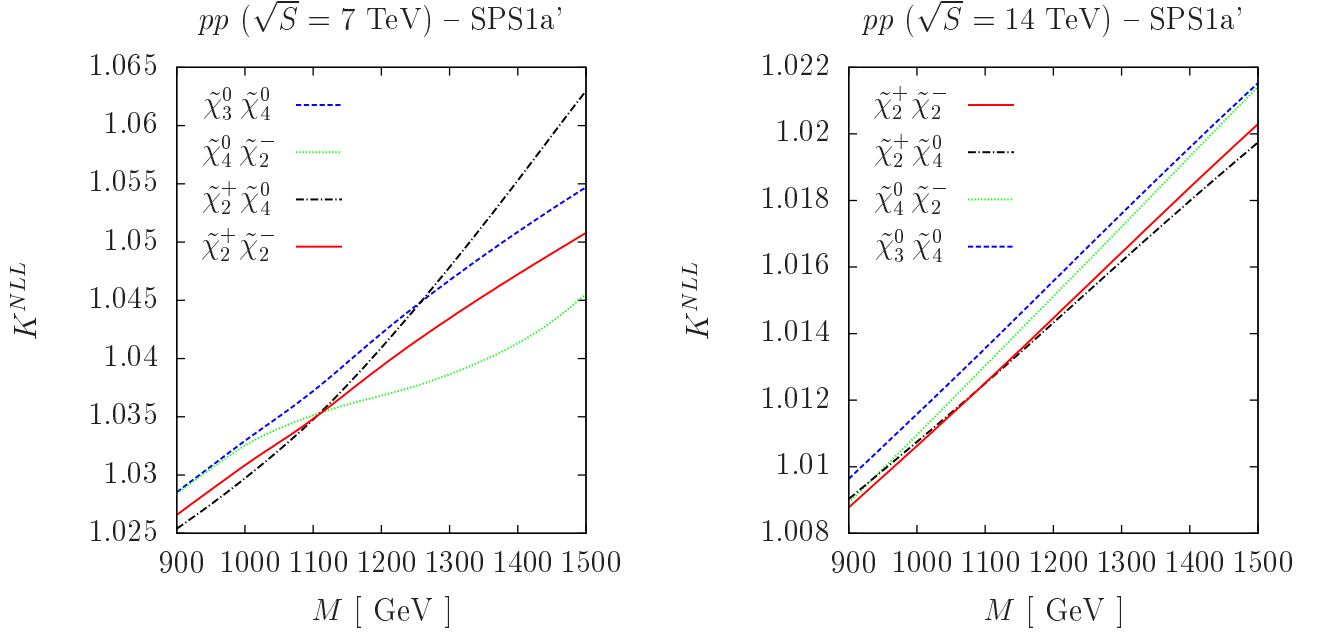


FIG. 15: Same as Fig. 14 for heavy gaugino pairs at the LHC with $\sqrt{S} = 7$ TeV (left) and $\sqrt{S} = 14$ TeV (right).

TABLE III: Total cross sections for the production of $\tilde{\chi}_1^+ \tilde{\chi}_2^0$ pairs in the SPS1a' scenario at different hadron colliders and center-of-mass energies in the LO, NLO and NLL+NLO approximation, together with the corresponding scale and PDF uncertainties.

Colliders	$\sigma^{\text{NLL+NLO}}$ [fb]	σ^{NLO} [fb]	σ^{LO} [fb]
$p\bar{p}(\sqrt{S} = 1.96 \text{ TeV})$	$30.9^{+0.1}_{-0.2} \text{ } ^{+1.5}_{-1.9}$	$31.2^{+0.9}_{-1.2} \text{ } ^{+1.5}_{-1.9}$	$27.2^{+3.6}_{-3.0}$
$pp(\sqrt{S} = 7 \text{ TeV})$	$263.3^{+0.6}_{-1.3} \text{ } ^{+11.4}_{-13.2}$	$265.5^{+5.0}_{-4.3} \text{ } ^{+11.5}_{-13.2}$	$223.1^{+6.9}_{-7.1}$
$pp(\sqrt{S} = 10 \text{ TeV})$	$470.7^{+1.4}_{-2.3} \text{ } ^{+17.7}_{-19.3}$	$474.0^{+8.3}_{-6.0} \text{ } ^{+17.7}_{-19.4}$	$387.4^{+2.5}_{-4.3}$
$pp(\sqrt{S} = 14 \text{ TeV})$	$772.7^{+1.6}_{-3.1} \text{ } ^{+25.5}_{-26.7}$	$777.5^{+11.9}_{-7.4} \text{ } ^{+25.5}_{-26.7}$	$623.7^{+4.7}_{-9.3}$

the one for $\tilde{\chi}_2^+ \tilde{\chi}_2^-$ pairs, and it is in fact not much smaller than the one for the considerably lighter gaugino-like $\tilde{\chi}_2^0 \tilde{\chi}_2^0$ pairs. In general, the heavy gaugino cross sections are, however, significantly smaller than those for light gauginos.

In Tab. V, we present finally total cross sections for the tripleton channel in our different benchmark scenarios at the LHC with its current center-of-mass energy of $\sqrt{S} = 7$ TeV. Since the masses of $\tilde{\chi}_1^\pm$ and $\tilde{\chi}_2^0$ are always rather similar, one expects also similar total cross sections. This is indeed confirmed by the $\sqrt{S} = 7$ TeV results in Tab. III and the numbers in Tab. V with the notable exceptions of LM7 and LM9, where the cross section is about a factor of two and one order of magnitude larger than for the other points, respectively. This is partly due to the lower gaugino masses at LM9 and partly to the much heavier squark masses, which suppress the t - and u -channels and thus their destructive interference with the s -channel amplitudes. The additional jet veto (JV), i.e. the rejection of events containing jets with transverse momentum $p_T > 20$ GeV, envisaged by the ATLAS collaboration to suppress the background from top quark pair production, has obviously no consequences at LO, since gauginos are exclusively produced at this order. An additional quark or gluon can only be present at NLO or NLL+NLO, and restricting its transverse momentum to low values reduces the total cross sections slightly with respect to the unrestricted predictions. The small reduction of the signal cross section in combination with a large reduction of the background should therefore indeed lead to a much better significance.

V. CONCLUSIONS

In summary, we presented in this paper a complete analysis of threshold resummation effects on direct light and heavy gaugino pair production at the Tevatron and at the LHC with its current, intermediate, and design center-

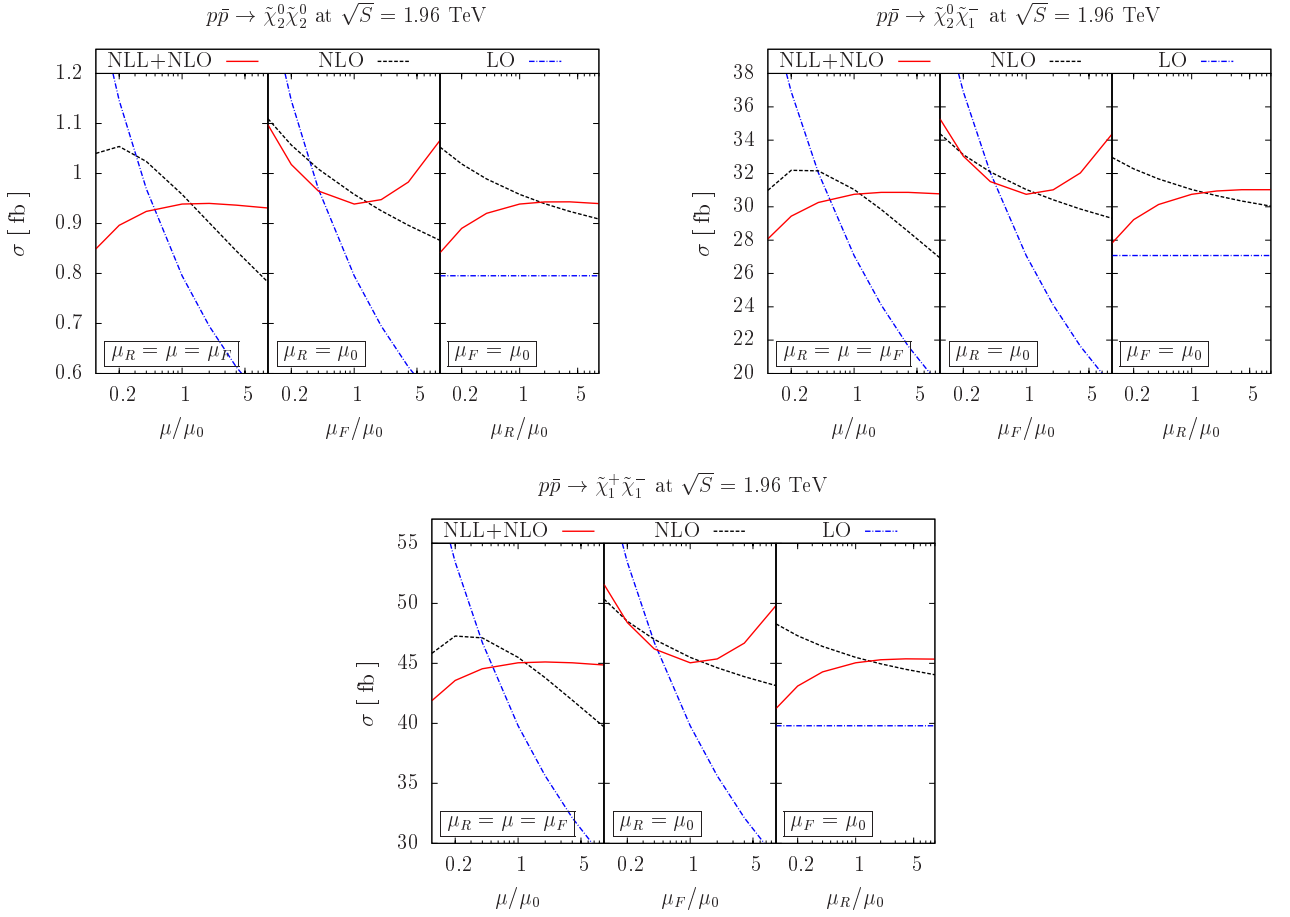


FIG. 16: Total cross sections for the production of neutralino (top left), chargino-neutralino (top right) and chargino pairs (bottom) at the Tevatron with $\sqrt{S} = 1.96$ TeV in the LO (blue, dot-dashed), NLO (black, dashed) and NLL+NLO (red, full) approximation.

of-mass energies. We confirmed the existing NLO calculation and extended it to include also mixing effects for intermediate squarks. Soft gluon radiation in the threshold region was resummed at leading and next-to-leading logarithmic accuracy into a Sudakov exponential, and the full SUSY-QCD corrections were retained in the finite coefficient function. This allowed us to correctly match the resummed cross section at NLL accuracy to the NLO perturbative cross section. Universal subleading logarithms coming from the splitting of initial partons were resummed in full matrix form, i.e. including also non-diagonal splittings. We found that resummation increased the invariant mass spectra and total cross sections only slightly, but stabilized the reorganized perturbative series considerably with respect to the fixed-order calculation. For future reference, we presented total cross sections with the corresponding theoretical errors from scale and PDF variations at LO, NLO and NLL+NLO in tabular form for several commonly used SUSY benchmark points, light and heavy gaugino pairs, and various hadron collider types and energies.

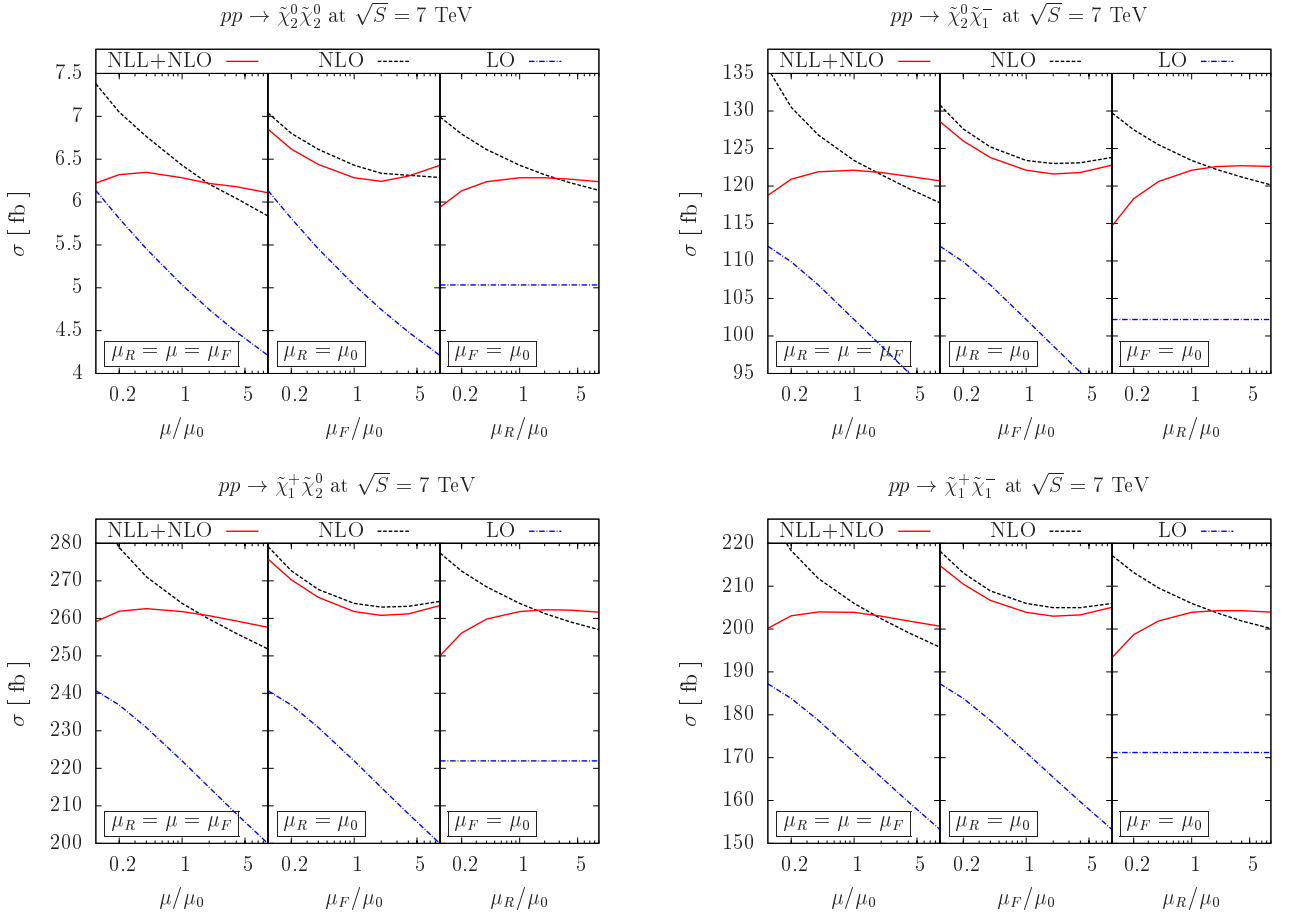


FIG. 17: Same as Fig. 16 for the LHC with its current center-of-mass energy of $\sqrt{S} = 7$ TeV.

Appendix A: Quark and squark couplings to weak gauge bosons and gauginos

The coupling strengths of the electroweak gauge bosons Z and W to left- and right-handed (s)quarks q (\tilde{q}) with weak isospin T_q^3 and fractional electric charge e_q are given by

$$\begin{aligned}
 \{L_{qqZ}, R_{qqZ}\} &= -\frac{1}{2c_W}(T_q^3 - e_q x_W), \\
 \{L_{\tilde{q}_i \tilde{q}_j Z}, R_{\tilde{q}_i \tilde{q}_j Z}\} &= -\frac{1}{2c_W}(T_q^3 - e_q x_W)\{R_{i1}^{\tilde{q}} R_{j1}^{\tilde{q}*}, R_{i2}^{\tilde{q}} R_{j2}^{\tilde{q}*}\}, \\
 \{L_{udW}, R_{udW}\} &= \left\{-\frac{V_{ud}}{2c_W}, 0\right\}, \\
 \{L_{\tilde{u}_i \tilde{d}_j W}, R_{\tilde{u}_i \tilde{d}_j W}\} &= \left\{-\frac{V_{ud}}{2c_W} R_{i1}^{\tilde{u}} R_{j1}^{\tilde{d}*}, 0\right\},
 \end{aligned} \tag{A1}$$

where $x_W = 1 - c_W^2 = s_W^2 = \sin^2 \theta_W$ is the squared sine of the electroweak mixing angle, $R_{ij}^{\tilde{u}, \tilde{d}}$ are the elements of the rotation matrices diagonalizing the up- and down-type squark mass matrices, and V_{ud} are the elements of the CKM

TABLE IV: Total cross sections for the production of various gaugino pairs in the SPS1a' scenario at the LHC with its design center-of-mass energy of $\sqrt{S} = 14$ TeV. The central predictions are given at LO, NLO and NLL+NLO together with the corresponding scale and PDF uncertainties.

Gaugino pair	$\sigma^{\text{NLL+NLO}}$ [fb]	σ^{NLO} [fb]	σ^{LO} [fb]
$\tilde{\chi}_2^0 \tilde{\chi}_2^0$	$25.1^{+0.3}_{-0.2} \text{ } ^{+1.2}_{-0.7}$	$25.5^{+0.8}_{-0.6} \text{ } ^{+1.3}_{-0.7}$	$19.2^{+0.3}_{-0.4}$
$\tilde{\chi}_1^+ \tilde{\chi}_1^-$	$665.8^{+1.0}_{-2.2} \text{ } ^{+20.6}_{-20.6}$	$671.1^{+10.8}_{-6.6} \text{ } ^{+20.7}_{-20.6}$	$533.4^{+3.4}_{-7.3}$
$\tilde{\chi}_2^0 \tilde{\chi}_1^-$	$433.3^{+0.6}_{-0.8} \text{ } ^{+17.9}_{-16.0}$	$436.9^{+7.2}_{-3.5} \text{ } ^{+17.9}_{-16.1}$	$348.3^{+2.2}_{-4.9}$
$\tilde{\chi}_1^+ \tilde{\chi}_2^0$	$772.7^{+1.6}_{-3.1} \text{ } ^{+25.5}_{-26.7}$	$777.5^{+11.9}_{-7.4} \text{ } ^{+25.5}_{-26.7}$	$623.7^{+4.7}_{-9.3}$
$\tilde{\chi}_3^0 \tilde{\chi}_4^0$	$14.6^{+0.0}_{-0.1} \text{ } ^{+0.7}_{-0.7}$	$14.8^{+0.3}_{-0.3} \text{ } ^{+0.7}_{-0.7}$	$12.1^{+0.5}_{-0.5}$
$\tilde{\chi}_2^+ \tilde{\chi}_2^-$	$14.0^{+0.1}_{-0.0} \text{ } ^{+0.7}_{-0.6}$	$14.2^{+0.3}_{-0.3} \text{ } ^{+0.7}_{-0.6}$	$11.7^{+0.5}_{-0.5}$
$\tilde{\chi}_3^0 \tilde{\chi}_2^-$	$8.5^{+0.0}_{-0.0} \text{ } ^{+0.6}_{-0.5}$	$8.6^{+0.2}_{-0.2} \text{ } ^{+0.6}_{-0.5}$	$6.9^{+0.3}_{-0.3}$
$\tilde{\chi}_2^+ \tilde{\chi}_3^0$	$19.1^{+0.1}_{-0.1} \text{ } ^{+0.9}_{-1.0}$	$19.3^{+0.4}_{-0.4} \text{ } ^{+0.9}_{-1.0}$	$16.0^{+0.7}_{-0.7}$
$\tilde{\chi}_4^0 \tilde{\chi}_2^-$	$7.8^{+0.0}_{-0.0} \text{ } ^{+0.5}_{-0.5}$	$7.9^{+0.2}_{-0.2} \text{ } ^{+0.5}_{-0.5}$	$6.4^{+0.3}_{-0.3}$
$\tilde{\chi}_2^+ \tilde{\chi}_4^0$	$17.7^{+0.1}_{-0.1} \text{ } ^{+0.8}_{-0.9}$	$17.8^{+0.4}_{-0.3} \text{ } ^{+0.8}_{-0.9}$	$14.9^{+0.7}_{-0.6}$

TABLE V: Total cross sections for the production of $\tilde{\chi}_1^+ \tilde{\chi}_2^0$ pairs at the LHC with its current center-of-mass energy of $\sqrt{S} = 7$ TeV for different SUSY benchmark points. The central predictions are given at LO, NLO and NLL+NLO together with the corresponding scale and PDF uncertainties.

Scenario	$\sigma^{\text{NLL+NLO}}$ [fb]	σ^{NLO} [fb]	σ^{LO} [fb]
LM1	$294.6^{+0.8}_{-1.4} \text{ } ^{+12.8}_{-14.5}$	$297.0^{+5.8}_{-4.8} \text{ } ^{+12.8}_{-14.5}$	$248.2^{+7.1}_{-7.5}$
LM7	$538.9^{+2.4}_{-3.5} \text{ } ^{+23.9}_{-26.7}$	$543.8^{+12.8}_{-10.7} \text{ } ^{+24.0}_{-26.8}$	$441.2^{+14.0}_{-14.3}$
LM9	$1736.2^{+8.0}_{-12.1} \text{ } ^{+68.8}_{-74.3}$	$1750.3^{+38.8}_{-28.8} \text{ } ^{+69.0}_{-74.4}$	$1374.4^{+8.4}_{-15.7}$
SU2	$171.7^{+0.5}_{-0.9} \text{ } ^{+8.5}_{-9.8}$	$173.4^{+4.2}_{-3.9} \text{ } ^{+8.5}_{-9.8}$	$145.0^{+7.4}_{-7.0}$
SU3	$116.9^{+0.1}_{-0.4} \text{ } ^{+5.6}_{-6.4}$	$118.0^{+2.2}_{-2.1} \text{ } ^{+5.6}_{-6.4}$	$101.6^{+4.6}_{-4.4}$
SU2+JV	$170.4^{+0.2}_{-0.7} \text{ } ^{+8.6}_{-9.8}$	$172.0^{+3.9}_{-3.6} \text{ } ^{+8.6}_{-9.9}$	$145.0^{+7.4}_{-7.0}$
SU3+JV	$115.4^{+0.1}_{-0.1} \text{ } ^{+5.6}_{-6.4}$	$116.6^{+1.9}_{-1.8} \text{ } ^{+5.6}_{-6.4}$	$101.6^{+4.6}_{-4.4}$

matrix. Their SUSY counterparts, i.e. the squark-quark-gaugino couplings, are given by

$$\begin{aligned}
L_{\tilde{d}_j d \tilde{\chi}_i^0} &= \frac{(e_d - T_d^3) s_W N_{i1} + T_q^3 c_W N_{i2}}{\sqrt{2} c_W} R_{j1}^{\tilde{d}*} + \frac{m_d N_{i3}}{2\sqrt{2} m_W \cos \beta} R_{j2}^{\tilde{d}*}, \\
R_{\tilde{d}_j d \tilde{\chi}_i^0} &= -\frac{e_d s_W N_{i1}^*}{\sqrt{2} c_W} R_{j2}^{\tilde{d}*} + \frac{m_d N_{i3}^*}{2\sqrt{2} m_W \cos \beta} R_{j1}^{\tilde{d}*}, \\
L_{\tilde{u}_j u \tilde{\chi}_i^0} &= \frac{(e_u - T_u^3) s_W N_{i1} + T_q^3 c_W N_{i2}}{\sqrt{2} c_W} R_{j1}^{\tilde{u}*} + \frac{m_u N_{i4}}{2\sqrt{2} m_W \sin \beta} R_{j2}^{\tilde{u}*}, \\
R_{\tilde{u}_j u \tilde{\chi}_i^0} &= -\frac{e_u s_W N_{i1}^*}{\sqrt{2} c_W} R_{j2}^{\tilde{u}*} + \frac{m_u N_{i4}^*}{2\sqrt{2} m_W \sin \beta} R_{j1}^{\tilde{u}*}, \\
L_{\tilde{d}_j u \tilde{\chi}_i^\pm} &= \frac{1}{2} \left[U_{i1} R_{j1}^{\tilde{d}*} - \frac{m_d U_{i2}}{\sqrt{2} m_W \cos \beta} R_{j2}^{\tilde{d}*} \right] V_{ud}, \\
R_{\tilde{d}_j u \tilde{\chi}_i^\pm} &= -\frac{m_u V_{i2}^* V_{ud}}{2\sqrt{2} m_W \sin \beta} R_{j1}^{\tilde{d}*}, \\
L_{\tilde{u}_j d \tilde{\chi}_i^\pm} &= \frac{1}{2} \left[V_{i1} R_{j1}^{\tilde{u}*} - \frac{m_u V_{i2}}{\sqrt{2} m_W \sin \beta} R_{j2}^{\tilde{u}*} \right] V_{ud}^*, \\
R_{\tilde{u}_j d \tilde{\chi}_i^\pm} &= -\frac{m_d U_{i2}^* V_{ud}^*}{2\sqrt{2} m_W \cos \beta} R_{j1}^{\tilde{u}*}, \tag{A2}
\end{aligned}$$

where the matrices N , U and V diagonalize the neutral and charged gaugino-higgsino mass matrices, $m_{u,d}$ are the up- and down-type quark masses, and m_W is the mass of the W -boson. All other couplings vanish due to electromagnetic charge conservation [1].

Acknowledgments

This work has been supported by a Ph.D. fellowship of the French ministry for education and research and by the Theory-LHC-France initiative of the CNRS/IN2P3.

-
- [1] H. P. Nilles, Phys. Rept. **110** (1984) 1; H. E. Haber and G. L. Kane, Phys. Rept. **117** (1985) 75; J. F. Gunion and H. E. Haber, Nucl. Phys. B **272** (1986) 1 [Erratum-ibid. B **402** (1993) 567].
- [2] E. Witten, Nucl. Phys. B **188** (1981) 513.
- [3] S. Dimopoulos, S. Raby and F. Wilczek, Phys. Rev. D **24** (1981) 1681.
- [4] J. R. Ellis, J. S. Hagelin, D. V. Nanopoulos, K. A. Olive and M. Srednicki, Nucl. Phys. B **238** (1984) 453.
- [5] V. Barger, R. Robinett, W. Keung and R. Phillips, Phys. Lett. B **131** (1983) 372; S. Dawson, E. Eichten and C. Quigg, Phys. Rev. D **31** (1985) 1581; D. A. Dicus, S. Nandi and J. Woodside, Phys. Rev. D **41** (1990) 2347; M. Klasen and G. Pignol, Phys. Rev. D **75** (2007) 115003.
- [6] G. Bozzi, B. Fuks and M. Klasen, Phys. Rev. D **72** (2005) 035016; D. Berdine and D. Rainwater, Phys. Rev. D **72** (2005) 075003; S. Bornhauser, M. Drees, H. K. Dreiner and J. S. Kim, Phys. Rev. D **76** (2007) 095020.
- [7] T. Gehrmann, D. Maitre and D. Wyler, Nucl. Phys. B **703** (2004) 147; G. Bozzi, B. Fuks and M. Klasen, Phys. Lett. B **609** (2005) 339; J. Debove, B. Fuks and M. Klasen, Phys. Rev. D **78** (2008) 074020.
- [8] G. Bozzi, B. Fuks, B. Herrmann and M. Klasen, Nucl. Phys. B **787** (2007) 1; F. del Aguila *et al.*, Eur. Phys. J. C **57** (2008) 183; B. Fuks, B. Herrmann and M. Klasen, Nucl. Phys. B **810** (2009) 266.
- [9] A. T. Alan, K. Cankocak and D. A. Demir, Phys. Rev. D **75** (2007) 095002 [Erratum-ibid. D **76** (2007) 119903].
- [10] W. Beenakker, R. Höpker, M. Spira and P. M. Zerwas, Nucl. Phys. B **492** (1997) 51; W. Beenakker, M. Krämer, T. Plehn, M. Spira and P. M. Zerwas, Nucl. Phys. B **515** (1998) 3; H. Baer, B. W. Harris and M. H. Reno, Phys. Rev. D **57** (1998) 5871; E. L. Berger, M. Klasen and T. M. P. Tait, Phys. Rev. D **59** (1999) 074024; E. L. Berger, M. Klasen and T. M. P. Tait, Phys. Lett. B **459** (1999) 165; E. L. Berger, M. Klasen and T. M. P. Tait, Phys. Rev. D **62** (2000) 095014 [Erratum-ibid. **67** (2003) 099901]; M. Spira, arXiv:hep-ph/0211145; L. G. Jin, C. S. Li and J. J. Liu, Eur. Phys. J. C **30** (2003) 77; L. G. Jin, C. S. Li and J. J. Liu, Phys. Lett. B **561** (2003) 135.
- [11] W. Beenakker, M. Klasen, M. Krämer, T. Plehn, M. Spira and P. M. Zerwas, Phys. Rev. Lett. **83** (1999) 3780 [Erratum-ibid. **100** (2008) 029901].
- [12] W. Hollik, M. Kollar and M. K. Trenkel, JHEP **0802** (2008) 018; W. Hollik, E. Mirabella and M. K. Trenkel, JHEP **0902** (2009) 002; E. Mirabella, JHEP **0912** (2009) 012.
- [13] G. Bozzi, B. Fuks and M. Klasen, Phys. Rev. D **74** (2006) 015001; M. Klasen, Nucl. Phys. Proc. Suppl. **160** (2006) 111; L. L. Yang, C. S. Li, J. J. Liu and Q. Li, Phys. Rev. D **72** (2005) 074026; H. K. Dreiner, S. Grab, M. Krämer and M. K. Trenkel, Phys. Rev. D **75** (2007) 035003; Y. Q. Chen, T. Han and Z. G. Si, JHEP **0705** (2007) 068; J. Debove, B. Fuks and M. Klasen, Phys. Lett. B **688** (2010) 208; J. Debove, arXiv:0908.4149 [hep-ph].
- [14] G. Bozzi, B. Fuks and M. Klasen, Nucl. Phys. B **777** (2007) 157; A. Kulesza and L. Motyka, Phys. Rev. Lett. **102** (2009) 111802; U. Langenfeld and S. O. Moch, Phys. Lett. B **675** (2009) 210; A. Kulesza and L. Motyka, Phys. Rev. D **80** (2009) 095004; W. Beenakker, S. Brensing, M. Krämer, A. Kulesza, E. Laenen and I. Niessen, JHEP **0912** (2009) 041.
- [15] G. Bozzi, B. Fuks and M. Klasen, Nucl. Phys. B **794** (2008) 46; B. Fuks, M. Klasen, F. Ledroit, Q. Li and J. Morel, Nucl. Phys. B **797** (2008) 322.
- [16] T. Aaltonen *et al.* [CDF Collaboration], Phys. Rev. Lett. **101** (2008) 251801; R. Forrest [CDF Collaboration], arXiv:0910.1931 [hep-ex]; V. M. Abazov *et al.* [D0 Collaboration], Phys. Lett. B **680** (2009) 34.
- [17] C. S. Li, Z. Li, R. J. Oakes and L. L. Yang, Phys. Rev. D **77** (2008) 034010.
- [18] G. Passarino and M. J. G. Veltman, Nucl. Phys. B **160** (1979) 151.
- [19] M. Böhm, A. Denner and H. Joos, *Gauge theories of the strong and electroweak interaction*. Teubner, Stuttgart (2001).
- [20] J. A. Aguilar-Saavedra *et al.*, Eur. Phys. J. C **46** (2006) 43.
- [21] S. Catani and M. H. Seymour, Nucl. Phys. B **485** (1997) 291 [Erratum-ibid. B **510** (1998) 503].
- [22] G. Sterman, Nucl. Phys. B **281** (1987) 310; N. Kidonakis and G. Sterman, Nucl. Phys. B **505** (1997) 321; N. Kidonakis, G. Oderda and G. Sterman, Nucl. Phys. B **525** (1998) 299.
- [23] G. Altarelli and G. Parisi, Nucl. Phys. B **126** (1977) 298.
- [24] W. R. Frazer and J. F. Gunion, Phys. Rev. D **19** (1979) 2447.
- [25] W. Furmanski and R. Petronzio, Z. Phys. C **11** (1982) 293.
- [26] A. M. Polyakov, Nucl. Phys. B **164** (1980) 171; G. P. Korchemsky and A. V. Radyushkin, Phys. Lett. B **171** (1986) 459.
- [27] S. Catani and L. Trentadue, Nucl. Phys. B **327** (1989) 323; S. Catani and L. Trentadue, Nucl. Phys. B **353** (1991) 183.
- [28] A. Vogt, Phys. Lett. B **497** (2001) 228.
- [29] M. Krämer, E. Laenen and M. Spira, Nucl. Phys. B **511** (1998) 523; S. Catani, D. de Florian and M. Grazzini, JHEP **0105** (2001) 025.
- [30] A. Kulesza, G. Sterman and W. Vogelsang, Phys. Rev. D **66** (2002) 014011; L. G. Almeida, G. Sterman and W. Vogelsang, Phys. Rev. D **80** (2009) 074016.
- [31] T. O. Eynck, E. Laenen and L. Magnea, JHEP **0306** (2003) 057.
- [32] R. Hamberg, W. L. van Neerven and T. Matsuura, Nucl. Phys. B **359** (1991) 343 [Erratum-ibid. B **644** (2002) 403].

- [33] H. Contopanagos and G. Sterman, Nucl. Phys. B **419** (1994) 77.
- [34] S. Catani, M. L. Mangano, P. Nason and L. Trentadue, Nucl. Phys. B **478** (1996) 273.
- [35] C. Amsler *et al.* [Particle Data Group], Phys. Lett. B **667** (2008) 1.
- [36] Tevatron Electroweak Working Group, arXiv:0903.2503 [hep-ex].
- [37] P. M. Nadolsky *et al.*, Phys. Rev. D **78** (2008) 013004.
- [38] W. Porod, Comput. Phys. Commun. **153** (2003) 275.
- [39] B. C. Allanach *et al.*, in *Proc. of the APS/DPF/DPB Summer Study on the Future of Particle Physics (Snowmass 2001)* ed. N. Graf, Eur. Phys. J. C **25** (2002) 113.
- [40] M. Battaglia, A. De Roeck, J. R. Ellis, F. Gianotti, K. A. Olive and L. Pape, Eur. Phys. J. C **33** (2004) 273.
- [41] G. Bayatian *et al.* [CMS Collaboration], J. Phys. G **34** (2007) 995.
- [42] G. Aad *et al.* [ATLAS Collaboration], arXiv:0901.0512.
- [43] At the tree-level, we neglect s -channel Higgs-boson exchanges, which may be produced by initial-state gluons through top-quark loops.
- [44] As it is customary, we absorb a factor of $(2\pi\mu_R)^{4-D}$ in the definition of the scalar integrals, where μ_R is the renormalization scale.
- [45] This is at variance with Ref. [17], where the quark wave functions are renormalized on-shell, thereby absorbing finite SUSY contributions into the definition of the quark fields.
- [46] For a comparison with Eq. (20) one must, of course, evaluate δZ_q in axial (not Feynman) gauge and recover the renormalization scale dependence through the replacement $\ln 4\pi \rightarrow \ln 4\pi\mu_R^2$.